

**Searching for correlations between vibrational spectral features and structural parameters
of silicate glass network**

Hongshen Liu,^{a+} Seung Ho Hahn,^{b+} Mengguo Ren,^c Mahadevan Thiruvillamalai,^c Timothy M.
Gross,^d Jincheng Du,^c Adri C. T. van Duin,^{a,b} and Seong H. Kim^{a,*}

^a Department of Chemical Engineering and Materials Research Institute, The Pennsylvania
State University, University Park, PA 16802, USA

^b Department of Mechanical Engineering, The Pennsylvania State University, University Park,
PA 16802, USA

^c Department of Material Science and Engineering, University of North Texas, Denton, TX
76203, USA

^d Corning Research and Development Corporation, Corning, NY 14831, USA

⁺ equal contributions

*Corresponding author: shk10@psu.edu

Abstract: Infrared (IR) and Raman spectroscopic features of silicate glasses are often interpreted based on the analogy with those of smaller molecules, molecular clusters, or crystalline counterparts; this study tests the accuracy and validity of these widely cited peak assignment schemes by comparing vibrational spectral features with bond parameters of the glass network created by molecular dynamics (MD) simulations. A series of sodium silicate glasses with compositions of $[\text{Na}_2\text{O}]_x[\text{Al}_2\text{O}_3]_2[\text{SiO}_2]_{98-x}$ with $x = 7, 12, 17,$ and 22 were synthesized and analyzed with IR and Raman. A silica glass substrate was also analyzed for comparison. Glass structures with the same compositions were generated with MD simulations using three types of potentials: fixed partial charge pairwise (Teter), partial diffuse charge potential (MGFF), and bond-order based charge transfer potential (ReaxFF). The comparison of simulated and experimental IR spectra showed that, among these three potentials tested, ReaxFF reproduces the concentration-dependence of spectral features closest to the experimentally observed trend. Thus, the bond length and angle distributions as well as Si- Q^n species and ring size distributions of silica and sodium silicate glasses were obtained from ReaxFF-MD simulations and further compared with the peak assignment or deconvolution schemes which have been widely used since 1970's and 1980's – (i) correlation between the IR peak position in the Si-O stretch region ($1050 - 1120 \text{ cm}^{-1}$) and the Si-O-Si bond angle, (ii) deconvolution of the Raman bands in the Si-O stretch region with the Q^n speciation, and (iii) assignment of the Raman bands in the $420 - 600 \text{ cm}^{-1}$ region to the bending modes of $(\text{SiO})_n$ rings with different sizes (typically, $n = 3 - 6$). The comparisons showed that none of these widely used methods is congruent with the bond parameters or structures of silicate glass networks produced via ReaxFF-MD simulations. This finding invokes that the adequacy of these spectral interpretation methods must be questioned. Alternative interpretations are proposed, which are to be tested independently in future studies.

1. Introduction

Silicate glass is the most widely used glass type among various oxide glass systems.¹ The structure of silicate glass is complicated due to distributions of network formers and modifiers which are functions of glass composition and thermal history, and all these parameters collectively impact physical and chemical properties of glass.²⁻⁵ Therefore, understanding structure of silicate glass is of critical importance. Frequently used experimental methods for structural analysis of silicate glass include nuclear magnetic resonance (NMR),^{6,7} x-ray and neutron scattering,⁸ and vibrational spectroscopy such as infrared (IR) and Raman.⁹⁻¹¹ NMR analysis provides the distribution of local connectivity such as Q^n species. X-ray and neutron scattering methods give radial or pair distribution functions among the nearest and next nearest atoms. IR and Raman spectroscopy probe vibrational modes of covalently bonded atoms. Among these, IR and Raman techniques are most readily available in many laboratories, and sample preparations for IR and Raman analyses are relatively simple.¹²⁻¹⁴ Therefore, IR and Raman could be a routine analytical tool in glass science if explicit spectral interpretation schemes are established.

The spectral interpretation for IR and Raman analysis of glasses have been studied since 1970's and 80's. Ignoring details in peak shape and intensity, it has been generally known that the bands centered at $\sim 1060\text{ cm}^{-1}$ and $\sim 780\text{ cm}^{-1}$ can be assigned to the asymmetric and symmetric stretching of the Si-O-Si (BO) bond, respectively; the band (mostly shoulder) around 950 cm^{-1} can be ascribed to the stretching of Si-OH or Si-O⁻ (NBO) groups; and the bands near $450 \sim 600\text{ cm}^{-1}$ are attributed to the bending of the Si-O-Si bond.¹⁵⁻¹⁷ These are established by comparing with vibrational spectra of crystalline equivalents or small molecules with similar covalent bonds.^{18-20 21}

However, when further details are considered, the interpretation of vibrational spectral features of glass is not straightforward.^{22, 23} The reason is that neither small molecules nor crystals can fully represent the vibrational modes of glass. Small molecules are isolated from each other, while the same molecular units are structurally connected in crystalline and glass networks; thus, molecules can vibrate independently, but the same structural units in the crystal and glass network cannot. Vibrations in the crystal and glass are collective motions of atoms across many structurally connected molecular units.²⁴ This makes the vibrational features of the same molecular units in the solid different from those of isolated small molecules.²⁵⁻²⁷

In addition, crystal has a long-range translational symmetry, while glass does not. Raman scattering can probe vibrational modes only near the center of the Brillouin zone for the crystalline solid, while it can detect all modes in the amorphous solid.²⁸ Because contributions from all collective vibrations appear in IR and Raman spectra of glass, local variations in bond angles and lengths of the structural units as well as the randomness in their connectivity make the absorption bands of glass extremely broad. Consequently, their maximum-intensity positions are shifted and their relative intensities are different from the spectrum of the crystalline counterpart with the same chemical composition.²⁹ This is the reason why the IR and Raman spectra of silica glass are quite different from those of quartz crystal (see Figure 1) even though both are composed of the stoichiometrically-identical SiO_4 tetrahedral units linked together through corner-sharing.

Even with these complexities, one can find certain interpretation rules that have been widely cited and used in the literature. In IR analysis, the maximum-intensity position of the absorption band attributed to the asymmetric BO stretch was often correlated to the angle of the Si-O-Si bond connecting two SiO_4 tetrahedral units.³⁰⁻³² This argument was based on the non-

central force constant model developed using small $(\text{SiO}_4)_n$ clusters in 1970's and 80's.^{30, 33}

However, recent molecular dynamics (MD) simulation studies showed that, for pure silica glass, the IR band position of the BO stretch near 1100 cm^{-1} correlates well with the weighted average of the Si-O bond lengths, but not with the Si-O-Si bond angles;^{34, 35} whether the same can be applied to silicate glass was not confirmed at that time (and is tested in this study).

In Raman analysis, the bands at the same wavenumber region have been deconvoluted with the Q^n speciation. For example, the component at 1200 cm^{-1} was assigned to Q^4 species, and $1100\sim 1050 \text{ cm}^{-1}$, $1000\sim 950 \text{ cm}^{-1}$ and $900\sim 850 \text{ cm}^{-1}$ were assigned to Q^3 , Q^2 , and Q^1 species, respectively;^{10, 22, 36} but theoretical justification for this approach is still lacking. In the Si-O-Si bending region, the bands at $\sim 430 \text{ cm}^{-1}$, $\sim 495 \text{ cm}^{-1}$ and $\sim 600 \text{ cm}^{-1}$ have been assigned to $(\text{SiO})_n$ rings with $n = 6, 4,$ and 3 , respectively, in the silicate network.^{37, 38} A density functional theory (DFT) calculation study showed that the peak position of 485 cm^{-1} matches with the theoretically predicted value for a four-membered ring;³⁹ but, this does not mean that other assignments are correct. It should be noted that the Raman peak shape and peak position of the molecular clusters from DFT-level can vary depending on the basis set and energy normalization factor used in calculations.⁴⁰⁻⁴²

In this study, we seek for correlations between the peak position and shape of the network vibrational bands, i.e. Si-O stretching and Si-O-Si bending, detected in IR and Raman analysis of glass, and the structural parameters of the glass network created using MD simulations. The parameters considered are the covalent bond length and angle distributions, Q^n speciation, and the $(\text{SiO})_n$ ring size distribution. A series of sodium silicate glasses with compositions of $[\text{Na}_2\text{O}]_x[\text{Al}_2\text{O}_3]_2[\text{SiO}_2]_{98-x}$ with $x = 7, 12, 17,$ and 22 were synthesized and analyzed with IR and Raman. A small amount of Al_2O_3 (2 mol.%) was added to avoid phase separation during the

glass forming; for simplicity, these glasses will be called ‘sodium silicate’ hereafter. Fused quartz was used as a reference for silica glass; crystalline quartz was also included as comparison. These compositions were chosen since the glass structure can be simulated with currently available potentials.^{23,43,44} In this work, we compared three potentials – a widely used non-reactive fixed partial charge pairwise Teter potential^{45,46} and two recently developed reactive force fields, bond-order based charge transfer ReaxFF potential⁴⁷ and partial diffuse charge Mahadevan-Garofalini force field (MGFF).^{48,49} From the comparison of theoretical IR spectra calculated from the model structures simulated with these three potentials, it was found that ReaxFF can reproduce the concentration dependence of spectral feature most closely to the experimentally observed trend. Thus, the structural parameters generated from the ReaxFF-simulated glass structures were compared with the previously mentioned three interpretation rules. The findings from these comparisons question the adequacy of the previous peak assignments or interpretations that are frequently found in the literature.

The organization of the paper is as follows. In Section 2, we describe details of the sample preparation, the IR and Raman measurements, the force fields considered for MD simulations, and the calculation of IR spectral features from MD simulations. The simulation details for the glass model construction are described in the Supporting Information. In Section 3.1, we fully describe how the IR and Raman spectral features of silica and sodium silicate glasses evolve as the sodium concentration increases from 0 mol.% to 22 mol.%. For direct comparison, the IR and Raman spectra of crystalline quartz are included. In this section, we also review some errors found in the literature discussing vibrational spectra of silicate glass and define key questions to be investigated by comparing with MD simulations. In Section 3.2, the MD simulation results obtained with three different force fields – Teter, MGFF, and ReaxFF –

are compared, which is necessary to choose the most appropriate force field for this study. Here, we also illustrate the IR spectral features originating from BO-only and NBO-only in the glass network to give a theoretical insight into the difference in their contributions to the overall spectrum. In Section 3.3, we investigate which bond parameter – especially, Si-O bond length vs. Si-O-Si bond angle – of the ReaxFF-MD generated glass network correlates better with the peak position of the Si-O stretch band in IR. In Sections 3.4 and 3.5, we examine the adequacy or validity of the previous peak assignments relating the Q^n species and the $(SiO)_n$ ring size distribution to the stretching and bending bands of Raman spectra, respectively. Then, the conclusion and perspective are summarized in Section 4.

2. Experiment and Simulation Methods

2.1. Experimental details

Glass sample preparation

A series of sodium silicate glasses were melted with compositions of $[Na_2O]_x[Al_2O_3]_2[SiO_2]_{98-x}$ with $x=7, 12, 17, 22$. The glasses were prepared with raw materials of sodium carbonate, calcined alumina (Almatis) and Berkeley fine sand (US Silica). Total mass of 2kg was mixed in a Turbula mixer and melted in covered Pt crucibles with volume of 1800 cubic centimeter at 1650°C for 12 hours. The molten glasses were poured on a stainless-steel plate with a 8 inch \times 8 inch dimension. Afterwards, the glasses were annealed at estimated annealing temperature for 6 hours and cooled down at a rate of 100°C/h. It should be noted that due to high melting temperature and large volume of batches, the glass formed upon pouring ended up with the top surface flat enough for optical analysis. The exact annealing point was obtained by the

fiber elongation method.⁵⁰ The glasses were then re-annealed at measured annealing points for 2 hours and cooled down with a rate of 1°C/min. The analyzed composition for each glass was carried out by x-ray fluorescence (XRF), which is listed in Table 1. The density was determined by the buoyancy method for each sample and shown in Table 1. The homogeneity – absence of phase separation – was confirmed by HF-etching followed by imaging with scanning electron microscope for two of the glass compositions (7 mol. % Na₂O and 12 mol. % Na₂O).⁵¹ There might be a sodium depletion layer at surface formed during the glass melting; but, the depletion layer depth is expected to be around 30 nm based on the previous literatures,^{52, 53} which is much smaller than the effective probe depth of IR and Raman analyses. Thus, its impact on the IR and Raman spectra would be negligible.

For vibrational spectral analyses, the glass samples were cut in dimension of ~2cm×~2cm×1.5cm by diamond saw with liquid coolant. The test specimen was selected with the optically smooth and flat surface in the center of the as-melted and poured glass sample. In addition, fused quartz coupon (Technical Glass Products, Inc., Painesville Township, OH, USA) and z-cut crystalline quartz coupon (MTI Corporation, Richmond, CA, USA) were purchased and used as reference samples. All test specimens were cleaned thoroughly with DI water (LabChem Inc., Zelienople, PA, USA), ethanol (VWR, Radnor, PA, USA), and acetone (Honeywell Burdick & Jackson, Muskegon, MI, USA). They were then treated in a UV-Ozone chamber for at least 20 minutes.

Infrared and Raman spectrum measurement

Specular reflection infrared (SR-IR) spectra were collected using a Bruker Hyperion 3000 Microscope (Bruker, Co., Billerica, MA, USA) with a 15° objective lens. The incident

angle for IR beam is approximately 20° . The measurements were performed on the as-melted surface of sodium silicate glass specimens in the mid-infrared range ($400\text{-}4000\text{ cm}^{-1}$). The spectra were collected and averaged over 400 scans with a resolution of 4 cm^{-1} . The spectrum of a clean gold surface with mirror finish was used as a reference. Based on the complex refractive index values for silica and silicate glass,²⁴ the probe depth is estimated to be around $600\text{-}630\text{ nm}$ in the Si-O-Si stretching mode region ($1030\text{-}1100\text{ cm}^{-1}$).¹⁵ Raman spectra were collected with a Horiba LabRam HR Evolution Raman spectrometer (Horiba Scientific, Piscataway, NJ, USA). The laser source used was 488 nm . The incident laser beam was polarized in the vertical direction and the Raman signal was collected in the vertical direction. Raman spectra were collected by averaging three spots for each sample with a resolution of 6 cm^{-1} . Because we are investigating changes in vibrational spectral features as a function of glass composition observed each vibrational spectroscopy technique and not comparing the absolute intensities of the IR and Raman bands for the same band, the difference in effective probe depth between IR and Raman is not important in this study.

2.2 Computational details

Empirical force field methods - ReaxFF, Teter, and MGFF

MD simulations were carried out with three different types of potentials – Teter,⁵⁴ MGFF,⁵⁵ and ReaxFF Si/O/H/Na parameterization⁴⁷ – and the most reasonable potential was chosen based on the comparison of theoretically-calculated infrared spectra with the experimental spectra. In the following, highlights of each potential are summarized and the reason for choosing these potentials is elucidated. The complete details, e.g. analytical form of potential function and implementations, of each potential can be found elsewhere.⁴⁵⁻⁴⁹

ReaxFF is a reactive potential that is capable of modeling condensed phases and reproducing material properties.⁵⁶⁻⁵⁸ This reactive potential employs a polarizable, geometry dependent charge calculation method using the electronegativity equalization method (EEM) which allows a physically realistic charge distribution within the system of interest. The polarization effect that can be delivered with the ReaxFF method is especially important to describe glass materials since the charge of each atom could be defined or characterized based on their local environment. The changes in the interatomic interactions alter the local structure as well as the strength of the bonds and consequently may shift the predicted IR spectra from the MD simulation results. On the contrary to the feasibility mentioned with ReaxFF, the polarization fluctuations would not be associated with the rigid ionic pair potentials like the Teter potential, which fixes the full or partial charges for each element in the system. Nevertheless, the Teter potential brought significant contributions in understanding glass structures and found to be reliable with great reproducibility of the structural features of sodium containing silicate glasses.⁵⁴ The MGFF potential, which was initially designed to simulate the dissociation and reaction of water over silica surfaces, have recently expanded its application to sodium silicate glass systems.^{48, 55} In the case of MGFF, the functional form of Coulombic terms is based on a diffuse charge on each atom that varies as a function of distance from the central atom. Also, the formulation includes the Wolf attenuation factor to handle the long-range interactions.

All three potentials possess different distinctive features and have advantages over one another. More importantly, these potentials use different method to take account of the charge contributions. For this reason, we found that these potentials could be suitable for a comparative study to reproduce IR spectra from MD simulations and evaluate the concentration dependence. Although the polarizable effects through ReaxFF could give advantages in improved description

of the charge transferability within glass network and of the local environment surrounding modifier ions, the charge calculation method (EEM) and the complex analytical form of ReaxFF gives lower computational efficiency (approximately ~10 times computationally expensive) compared to Teter and MGFF potentials. For this reason, the scalability used in this study varies among different methodology: ReaxFF with the system size of 3040 atoms and Teter and MGFF with 6080 atoms with glass composition of $[\text{Na}_2\text{O}]_x[\text{Al}_2\text{O}_3]_2[\text{SiO}_2]_{98-x}$ with $x=7, 12, 17, 22$.

MD simulation details for predicting the IR spectra

MD simulations were carried out to probe the structural and vibrational properties of sodium silicate glasses. Different composition of the ternary system was modeled by varying the soda (Na_2O) content from 7, 12, 17, and 22 mol.%, while maintaining the alumina (Al_2O_3) composition the same (2 mol.%) for all cases. The sodium silicate glass system (7, 12, 17 and 22 mol.% Na_2O) used in this study was constructed by the melt-and-quench method where the details can be found in the Supporting Information.

To investigate the composition dependence on the IR spectra, the glass models were equilibrated at 300 K with ReaxFF, Teter and MGFF potentials and the trajectories and charge information was collected at an interval of 1 fs. Based on the trajectories, the total dipole moment of the system was calculated on-the-fly and these data were post-processed to derive the autocorrelation function of the derivative of total dipole moment. In the previous publication by Luo *et al.*,³⁴ the IR spectra of pure silica was successfully reproduced based on the Fourier transform of this autocorrelation function. The same approach has been employed in this study to generate the IR spectra of the sodium silicate glass from the MD simulations. Further details of

the data analysis process can be found in the recent publication as well as in the Supporting Information.³⁴

The MD simulation runs to produce IR spectra herein were carried out with the LAMMPS package.⁵⁹ While the simulations were performed with the periodic boundaries, the trajectories were collected with unwrapped atom coordinates to consider the atoms moving across the boundaries during the data production run. All simulations with Teter and MGFF potentials employed an integration time step of 1 fs, whereas smaller time step of 0.25 fs was used for ReaxFF MD simulations in order to properly observe the charge transfer between adjacent atoms along the trajectory. We implemented the recently developed Si/O/H/Na ReaxFF force field⁴⁷ with the Al interaction terms integrated from the parameterization of Pitman *et al.*⁶⁰

3. Results and Discussion

3.1 IR and Raman spectra of silica and sodium silicate glasses

The SR-IR and Raman spectra of silica (modeled with fused quartz) and a series of sodium silicate glasses with the Na₂O concentration of 7, 12, 17, and 22 mol.% are shown in Figure 1. For comparison, the spectra of crystalline quartz are also included. The spectral regimes of Si-O-Si bending and Si-O stretching are marked with green and yellow backgrounds, respectively, in Figure 1. In IR spectra (Figure 1a), the band in the 1088-1123 cm⁻¹ region is typically attributed to the asymmetric BO stretch.^{15, 16, 61} Sometimes, it was called the asymmetric stretch of the SiO₄ unit in analogy with the asymmetric stretch mode of a tetrahedral shape molecule (like the T₂ mode of the T_d symmetry group);^{9, 62} but, this is not appropriate because, unlike the isolated molecules, the inter-connection of SiO₄ units in the amorphous network distorts individual moieties from the perfect tetrahedral geometry and their vibrations

are concerted motions of these highly-connected SiO_4 units. The maximum intensity position of this band is 1123 cm^{-1} for fused quartz and gradually shifts to lower wavenumbers as the sodium concentration increases (from 1113 cm^{-1} for 7 mol.% Na_2O to 1088 cm^{-1} for 12 mol.%).

The reflection intensity of this band also decreases from 75% reflection for fused quartz to ~30% for the silicate glass with 22 mol.% Na_2O . The reflection intensity is not the same as the absorptivity.^{24, 63} The decrease of this band intensity has been attributed to the decrease of number of BOs or Q^4 species in the glass network as the network modifier ion (sodium) concentration increases. Although the NBO stretch band at $\sim 950\text{ cm}^{-1}$ grows as a result of increasing the sodium concentration,^{23, 64} its intensity increase does not mirror the magnitude of the intensity decrease of the BO stretch band at $1088 - 1123\text{ cm}^{-1}$ region. In other word, the total intensity is not conserved, while the NBO+BO amount and Q^n speciation are conserved (see Table 2 and Figure 6 in Section 3.4). This discrepancy has not been fully explained.

In IR, the shoulder at $\sim 1230\text{ cm}^{-1}$ is prominent for silica and decreases as the silica content decreases in the glass. For this reason, this shoulder is often thought to be characteristic of a silica-like structure.^{15, 65, 66} In some literatures, it was attributed to the longitudinal optical (LO) mode of silica;^{36, 67, 68} but its origin in amorphous glass is not still well understood. Note that a similar mode is also observed for soda lime silicate glass at high incidence angles of IR and its polarization dependence does not meet with the LO mode property.¹⁵

A completely opposite trend is observed in the Raman spectra of the same series (Figure 1b). The Raman band in the asymmetric BO stretch region is the weakest for silica and grows and shifts to higher wavenumbers as the sodium concentration increases. Based on the intensity growth with increasing sodium concentration, this band has been attributed to the stretching vibration of the silica tetrahedra with one NBO, i.e. Q^3 species.¹⁰ At a first glance, this appears

reasonable because the Raman intensity normally follows the Beer-Lambert law; but the trouble is that, if this interpretation is right, the small but noticeable intensity of the 1058 cm^{-1} band for silica must mean the presence of a considerable amount of Q^3 species in pure stoichiometric silica which is known to consist of Q^4 species with a negligible amount of Q^3 defects.

In contrast to the asymmetric BO stretch band, the symmetric BO stretch band ($\sim 750\text{ cm}^{-1}$ in IR and $\sim 800\text{ cm}^{-1}$ in Raman) shows only minute dependence on the sodium concentration. In the case of isolated T_d -symmetry molecules, the symmetric A_1 stretch mode is IR-inactive and Raman-active, while the asymmetric T_2 stretch mode is IR active and Raman-inactive.⁶⁹ One can see that in the silica spectra, the 750 cm^{-1} symmetric stretch band is much smaller than the 1123 cm^{-1} asymmetric stretch band in IR, while the 800 cm^{-1} symmetric stretch band is slightly larger than the 1058 cm^{-1} asymmetric stretch band. The relative intensities of these two bands in each spectrum appears to be reasonable when one considers the symmetry rules of the SiO_4 unit. However, the 750 cm^{-1} intensity in IR and the 800 cm^{-1} intensity in Raman do not decrease, while the SiO_4 (Q^4) fraction in the glass varies substantially as the sodium concentration increases from 7 mol.% to 22 mol.%. For crystalline quartz (Figure 1), the 750 cm^{-1} band is very strong in the IR spectrum (where the A_1 mode of the T_d symmetry must be inactive) and the 800 cm^{-1} band is extremely small in the Raman spectrum (where the A_1 mode is symmetry-allowed). These comparisons show that the symmetric stretch of BO in the glass network should not be viewed as the symmetric stretch of the isolated T_d symmetry molecule.

The bending vibration bands are in the $300 - 630\text{ cm}^{-1}$ for both IR and Raman spectra. In IR spectra, the 480 cm^{-1} band intensity decreases as the sodium concentration increases. The change in IR peak position is very minor (only 3 cm^{-1} while the sodium concentration increases from 0 to 22 mol.%). On the other hand, there are drastic changes in the bending vibration region

in Raman spectra. As the sodium concentration increases, the most dominant band of silica at 424 cm^{-1} decreases and shifts slightly to $\sim 450\text{ cm}^{-1}$; the relatively sharp peak at 480 cm^{-1} also decreases and slightly shift to $\sim 500\text{ cm}^{-1}$ at $[\text{Na}_2\text{O}] = 17\text{ mol.}\%$ and become indiscernible at $[\text{Na}_2\text{O}] = 22\text{ mol.}\%$; and the intensity in the $500 - 600\text{ cm}^{-1}$ region increases significantly and becomes a distinct band at 529 cm^{-1} when $[\text{Na}_2\text{O}]$ reaches $22\text{ mol.}\%$. It is difficult to determine if the 600 cm^{-1} band of silica, which is often assigned to the three-membered $(\text{SiO})_3$ ring,³⁸ is increasing or simply becoming broader and indistinguishable from the broad tail of the newly growing 529 cm^{-1} band.

3.2 Choosing proper potential for MD simulations

It is well known that glass properties simulated with MD can vary depending on the choice of potential functions describing inter-atomic interactions.^{70, 71} Because the prime interest of this study is spectral features and the IR spectrum can be obtained from the autocorrelation of polarization fluctuations of the simulated structure,^{34, 35, 72} we compared the SR-IR spectra calculated with different potentials with the experimental spectra shown in Figure 1a to choose the most appropriate one for further in-depth analysis. At this moment, obtaining the Raman spectrum from MD-simulated structures is quite difficult,⁷² so we did not use the Raman spectra in Figure 1b for comparison.

Figure 2 compares the SR-IR spectra of the glasses with the same compositions as the experimental samples in Figure 1 using the structures simulated with Teter, MGFF, and ReaxFF potentials. With the Teter potential (Figure 2a), the calculated stretching vibration band appears in the region significantly lower than the experimental value, and the position of the bending

vibration band is higher than the measured value. Also, the stretching band intensity is smaller than the bending intensity, which is opposite to the experimental data (Figure 1a). Thus, it can be concluded that the MD simulation results from the Teter potential would be inadequate to describe the structural features of glass that are relevant to the vibrational spectra. It is known that the partial charge pairwise Teter potential can generate reasonable short and medium range structure as compared to experiments for sodium silicate glasses and as a result it has been widely used in the structural studies of silicate glasses.^{54, 73-76} However, the fixed charge potential does not take into ion polarization effect which plays an important role in the vibrational spectra of the glass networks. It has been shown previously that including polarization can significantly improve the peak position and relative intensity of silica glass.⁷⁷

In MGFF-MD simulations (Figure 2b), the calculated stretching band is closer to the experimental result. But the bending vibration band position is a bit higher than the experimental values (Figure 1a). The intensity of the bending vibration band at 530 – 560 cm^{-1} is still higher than the stretching vibration band. Also, there is an additional band at $\sim 700 \text{ cm}^{-1}$, which cannot be matched with the experimental data. For these reasons, the MGFF-MD simulation results may not be accurate to use for spectral data interpretation.

In the ReaxFF-MD simulation, although detailed peak shapes are still different, the calculated vibrational band positions and relative intensities (Figure 2c) are in qualitative agreement with the experimental data (Figure 1a). The bending band intensity is smaller than the stretching band intensity. The Si-O stretching band appears at 1088 – 1113 cm^{-1} and the Si-O-Si bending band is around 470 – 510 cm^{-1} for the sodium silicate glass series with the compositions same as the experimental samples. As the sodium ion concentration increases, the stretching band is gradually red-shifted, which is congruent with the experimental data. Some differences

of the ReaxFF-MD simulation results (Figure 2c) from the experimental spectra (Figure 1a) may be the consequence of dealing with the limited number of atoms ($N=3040$) in the simulation box. Overall, it can be concluded that, among three potentials tested in this study, the ReaxFF potential produces the IR spectra most comparable to the experimental result. It is thus chosen for further study of searching.

In simulations, it is possible to calculate separate spectral contributions from BOs only and NBOs only. For this purpose, we analyzed the glass structures and updated trajectories by differentiating and registering every oxygen within the glass as BO or NBO based on the Si-O bond cutoff value of 2.1 Å. Then, IR spectra were calculated from the dipole moment fluctuations of the updated trajectories accounting for BOs only or NBOs only. This provides information of how vibrations of BOs and NBOs in the glass network contribute to the overall spectrum. It is found that the differences between the BO-only spectra (Figure 3a) and the full spectra (Figure 2c) are very minute. This is probably because BOs are the major components in the glass network in the concentration regime considered in this study. The only easily discernable difference is that the BO-only spectrum (Figure 3a) has a slightly lower intensity in the region below 350 cm^{-1} than the full spectrum (Figure 2c).

On the other hand, it is found that the features of the NBO-only spectra are quite different from those of the BO-only. First of all, the stretch band position of NBO is red-shifted compared to that of BO. This is somewhat congruent with the experimental data, although the calculated NBO peak positions ($1000\sim 1020\text{ cm}^{-1}$) are a bit higher than typical peak position for this species ($\sim 950\text{ cm}^{-1}$) used in the interpretation of experimental spectra.

In the bending region, the NBO-only spectra show two components. The higher wavenumber component position ($440\sim 460\text{ cm}^{-1}$) is slightly lower than the BO bending band

position (470~510 cm^{-1}) and the lower wavenumber component is centered at $\sim 230 \text{ cm}^{-1}$. This lower wavenumber band is not observed in experiments because most Fourier-transform infrared spectrometers are equipped with a KBr beam splitter and this cuts off the IR power below 400 cm^{-1} . This secondary component is probably responsible for the higher intensity below 350 cm^{-1} in the full spectra (Figure 2c) compared to the BO-only spectra (Figure 3a).

3.3 Can the Si-O stretch bands in IR be related to bond length or bond angle?

Based on the non-central force constant concept which allows the force constant (k) of the Si-O stretching mode to vary with a simple trigonometric function of the Si-O-Si bond angle (θ),^{30, 33, 78} the asymmetric BO stretch band position (ω_{as}) has often been related to the change in the angle of the Si-O-Si bond connecting two SiO_4 tetrahedral units.^{31, 79} Although it conceptually makes sense that the deviation of the Si-O-Si bond angle from the optimum value may weaken the Si-O bond energy, there has been no a priori explanation or justification for the simple trigonometric relationship between k and θ at the electronic structure level. A planar ring structure model was assumed in the non-central force constant model;⁷⁸ but, all rings identifiable in the silicate network are puckered (see Figure 7 in Section 3.5). In addition, it remains to be tested if the calculation for the isolated cluster model can be extended to the glass network, because the vibration of three-dimensionally connected random networks cannot be the same as the vibration of isolated small molecules in the gas phase. In computational studies for pure silica glass, it has been shown that the correlation between ω_{as} and θ could be positive or negative depending on the physical parameter affecting θ .³⁴ This may suggest that there is no theoretical reason that θ and ω_{as} are directly related as the cause and consequence with a single governing

relationship. Instead, it was shown that the intensity-averaged ω_{as} value of silica could be correlated linearly to the weighted-average of the Si-O bond length (d) distribution.³⁴ Inspired by these prior studies, we have checked if the intensity-averaged ω_{as} value of sodium silicate correlates with the distribution of d or θ .

Figure 4 displays the distributions of Si-BO and Si-NBO bond length as well as Si-O-Si bond angle in the silica and sodium silicate glasses simulated with ReaxFF-MD. In general, the most-probable bond length of Si-BO is longer than that of Si-NBO by ~ 0.02 Å. The bond length distributions of both Si-BO and Si-NBO shift to longer distances as the sodium concentration increases. These results are consistent with previous MD simulation results using a different potential.^{71, 80, 81} It should be noted that because of the sample history dependence of glass structure, which is the thermodynamically unavoidable complication of the non-equilibrium state, the change in bond parameter distributions may vary differently depending on the conditions imposed to the glass network. This was shown in our previous MD simulations for silica glass;³⁵ the Si-O stretch peak position always shows negative correlations with the weighted average value of the Si-O bond length distribution regardless of the physical constraints applied to the glass, while its correlation with the weighted average value of the Si-O-Si bond angle distribution varies from positive to negative depending on the physical constraint applied. This may suggest that the Si-O-Si bond angle change may not be the primary cause for the vibrational peak position; it might be a consequence governed by a secondary mechanism. As shown in the insets of Figures 4a and 4b, the Si-BO length distribution becomes broader upon the addition of sodium modifier ions, but the width of the Si-NBO length distribution remains relatively unchanged. In contrast, the Si-O-Si bond angle distribution shifts to lower angles as the sodium concentration increases (Figure 4c).

Figure 5 plots the intensity-weighted average position of the experimentally-measured asymmetric BO stretch band of the SR-IR spectra of sodium silicate glasses (Figure 1a) against the weighted average of the all Si-O bond length distribution, the Si-BO bond length distribution, and the Si-O-Si bond angle distribution obtained from ReaxFF-MD simulations (Figure 4). The data clearly show that the asymmetric BO stretch peak position correlates linearly with the Si-O or Si-BO bond length, but the correlation with the Si-O-Si bond angle is highly non-linear (or poor). The linear correlation between the asymmetric BO stretch peak position and the bond length has been tested and explained through a simplified vibrational normal mode analysis for a single SiO₄ cluster.³⁴ The data presented in this study confirms that the same trend or correlation is valid for sodium silicate glass too. Here, we do not suggest that the change in the bond length distribution is the only factor governing the shift of the BO stretch peak. Other bond parameters may also change as the sodium concentration increases in the glass; but they do not correlate with the peak shift as well as the weighted average of the Si-O bond length distribution does.

In the SR-IR analysis, it is important to note that the peak intensity or area is not directly proportional to the concentration of absorbing species or functional groups. The SR-IR intensity is fundamentally different from the absorbance (A) which is proportional to the concentration of species of interest through the Beer-Lambert law, $A = a \cdot b \cdot c$ where a is the absorptivity, b is the path length or probe depth, and c is the concentration of analyte. In theory, the SR-IR data can be processed with the Kramers-Kronig algorithm to the complex refractive index, $n + ik$, and the imaginary term (k) can be converted to the absorptivity ($a = 4\pi k/\lambda$ where λ is the wavelength).^{63,}
⁸² In practice, this conversion is mathematically complicated when the incidence angle is off the surface normal direction and its accuracy is often affected by experimental measurement errors or limitations.²⁴

One possible reason for the decrease in the SR-IR intensity upon increasing the modifier concentration could be associated to the broadness of the band in the spectra. In addition to the distributions in bond parameters of the structural units (Figure 4), the broadness of the absorption (resonance) band could also be caused by non-irradiative energy dissipation processes;⁸³⁻⁸⁵ if such inhomogeneous line broadening process exist, then the re-emission efficiency of the absorbed photon energy (which is defected as the reflectance) will decrease. Most silicate glasses with high concentrations of modifier ions have broader absorption bands and smaller k values than silica in the mid-IR region.²⁴

3.4 Can the Si-O stretch bands in Raman be related to Qⁿ speciation?

Based on the fact that the increase of sodium concentration in the sodium silicate glass will increase the Si-NBO fraction,⁸⁶ the growth of the Raman band in the 1050 – 1200 cm⁻¹ region has been attributed to the increase in the Q³ species concentration.^{36, 87-89} In the literatures interpreting the Si-O stretch spectral features in this way, the Raman bands were often deconvoluted into four components: Q⁴ species at 1200 cm⁻¹, Q³ species at 1050~1100 cm⁻¹, Q² species at 950~1000 cm⁻¹, and Q¹ species at 850~900 cm⁻¹.¹⁰ This argument was made based on the comparison of Raman spectra of silica, disilicate, metasilicate, and pyrosilicate glasses with the structures of their crystalline counterparts.^{36, 90}

To test the validity of this approach, we have obtained the Qⁿ speciation of the sodium silicate glass from ReaxFF-MD simulations. Table 2 summarizes the oxygen speciation in the sodium silicate glass obtained from ReaxFF-MD simulations. All oxygen atoms in the simulation box could be grouped as Si-BO, Si-NBO, and Si-O-Al. The amounts of Al-O-Al and Al-NBO

are negligible (<0.2% which are defects in the simulation). As expected, most sodium ions (modifier ions) are associated with Si-NBO. The small difference between the Si-NBO atom.% in the simulation and the Na mol.% in the composition is due to the charge compensation of the AlO_4 species in the glass network by sodium ions. The resulting Q^n speciation is plotted as a function of sodium concentration in Figure 6. The simulated result is in good agreement with the relative amount of Q^n species calculated based on the charge compensation principle using the actual composition of the glass determined from the XRF analysis (Table 1) [see the Supporting Information for calculation details]. The result is also congruent with the previously reported Q^n speciation based on NMR analysis.⁹⁰

If one compares the Raman peak shape and intensity in Figure 1b with the distribution of Q^n species in Figure 6, some inconsistency can be found. In the Raman spectrum of silica, the 1058 cm^{-1} peak is larger than the 1200 cm^{-1} peak although silica is composed of all Q^4 species and has negligible quantity of the Q^3 species. As the sodium concentration increases in the glass, the Q^3 species increases while the Q^4 species decreases. If one argues that the growth of the $1050\text{--}1100\text{ cm}^{-1}$ peak correlates with the increased concentration of the Q^3 species, then how could the change in the 1200 cm^{-1} Raman peak be related to the decrease of the Q^4 species in the glass structure? The 1200 cm^{-1} component does not decrease with increasing sodium concentration, instead its intensity grows as a shoulder of the main peak at $1050\text{--}1100\text{ cm}^{-1}$. Thus, the relative intensities of the deconvoluted components cannot be directly matched with the Q^n speciation.

More realistic interpretation could be proposed from the phonon density of state concept.^{91, 92} The quartz crystal has two Raman-active modes at 1068 cm^{-1} and 1163 cm^{-1} ; but

their signal intensities are extremely weak.⁹³ Computational studies of the phonon density of state for amorphous silica predicted that there are two modes of SiO₄ stretch in the 1050 – 1200 cm⁻¹ region and the lower one corresponds to the asymmetric Si-BO stretch.⁷⁰ The weak Raman bands of silica at 1058 cm⁻¹ and 1200 cm⁻¹ (Figure 1b) could correspond to these two modes. We speculate if the asymmetric vibrations involving SiO₄ (Q₄) groups become more active and the split of these band becomes smaller as the Q³ concentration increases and the network connectivity decreases; if so, that may explain the trend observed in Figure 1b. A similar phenomenon is well known in the Raman analysis of graphene. The ring breathing mode (D band) of the hexagonal *sp*² lattice is negligible in the Raman spectrum of defect-free graphene but becomes significant as the defect density increases and the *sp*² connectivity decreases.^{94, 95}

3.5 Can the bending vibration band in Raman be related to the (SiO)_n ring size of the silicate network?

For the bending mode region, the Raman peaks of glass have often been assigned to the (SiO)_n rings with different sizes (*n*) in the randomly-connected silicate glass network. Especially, the peaks at ~430 cm⁻¹, ~495 cm⁻¹ and ~600 cm⁻¹ have been assigned to six-, four-, three-membered rings (*n* = 6, 4, and 3), respectively.^{37, 38} In the experimentally measured Raman spectra of silica and sodium silicate glass series (Figure 1b), the broad band at ~430 cm⁻¹ and the sharp peak at ~495 cm⁻¹ decrease in intensity, while the components at ~530 cm⁻¹ and ~600 cm⁻¹ increase as the sodium concentration increases. If one uses the previous ring size assignment scheme, then the data could mean that the six- and four-membered ring fractions decrease, while the three-membered ring portion increases with the sodium modifier ion addition into the glass. Whether this interpretation is reasonable or not can be tested by comparing with the ring size

distribution in the glass structure with the same experimental composition obtained with ReaxFF-MD simulations.

The distribution of $(\text{SiO})_n$ rings in the silica and sodium silicate glass structures simulated with ReaxFF-MD is shown in Figure 7a. Examples of three-, six-, and ten-membered rings ($n = 3, 6, \text{ and } 10$, respectively) are shown in Figure 7b-7d. The ring size distribution becomes broader and shifts to larger rings as the sodium concentration increases. Intuitively, this makes sense; when a modifier ion breaks the Si-O-Si bond of a $(\text{SiO})_n$ ring, the resultant fragment will become a part of a larger ring. In the silica structure, the rings with $5 \leq n \leq 8$ are dominant. As the sodium modifier concentration increases, the relative abundances of rings with $n = 6$ and 7 decrease substantially and those of rings with $n \geq 9$ increase significantly.

When the ring size distribution (Figure 7a) is compared with the relative intensity variation with the sodium concentration in the Raman spectra (Figure 1b), it is obvious that the data cannot be explained with the ring size dependence of the peak position. Although the 600 cm^{-1} peak intensity can be seen clearly as a sharp peak for silica and a shoulder for sodium silicate glasses (Figure 1b), the three-membered ring population is negligible (Figure 7a). In the Raman spectra, the $\sim 495 \text{ cm}^{-1}$ peak is disappearing (Figure 1b), while the four-membered ring population does not change substantially (Figure 7a). The non-central force constant model predicted that the bending vibration peak position decreases with increasing ring size;⁷⁸ then what would be the ring size for the component growing in the region between $\sim 495 \text{ cm}^{-1}$ and 600 cm^{-1} with increasing sodium concentration (Figure 1b)?

In order to find the effect of sodium ions on the ring structure, the Si-O bond length and Si-O-Si bond angle of each n ring are plotted in Figure 8. At the first glance, one may notice that

the Si-O-Si bond angle of the three-membered ring is much smaller than other abundant rings with $n \geq 5$ and its Si-O bond length fluctuates a lot with the variation of sodium concentration. Its small bond angle is quite similar to the value calculated for the $(\text{HO})_3\text{Si-O-Si}(\text{OH})_3$ in which the hydrogen bonding interactions between two terminal OH groups cause more bending the Si-O-Si bond (see Table S4 in the Supporting Information). The large fluctuation in the Si-O bond length must be related to the fact that this small ring is not stable. As shown in Figure 7a, the population of the three-membered ring is negligible. So, the large deviation of its bond parameters from the most probable values would not make any impact on the overall energy and vibrational spectral feature.

For the rings with $n = 5 \sim 9$ that compose most of the network, the average Si-O-Si bond angles are close to the values expected for the structure where two adjacent SiO_4 units are not attracting each other (see Table S4 in the Supporting Information). Although variances are small, it is noticed that as the sodium concentration increases, the average Si-O bond length of each ring increases (Figure 8a) and the average Si-O-Si bond angle of the ring decreases (Figure 8b). This is manifested as the shift in the Si-O bond length distribution to the longer side (Figure 4a) and the Si-O-Si bond angle distribution of the lower side (Figure 4c). These changes must be the direct consequences of replacing covalent Si-BO bonds with more ionic Si-NBO bonds and sodium ions in the glass network. Similar to the correlation between the Si-O bond length distribution and the peak position of the Si-O stretch mode (Figure 5), it is expected that the change in the Si-O-Si bond angle distribution would also affect the position and shape of the Si-O-Si bend mode. But due to complex changes in the band shape (Figure 1b), it is difficult to find a simple empirical correlation as in the case of the Si-O stretch band (Figure 5).

The larger rings with $n \geq 10$ appear to have slightly longer bond lengths and smaller angles. But their populations are relatively small, and their backbones are often cross-linked to smaller size rings; thus, the importance of these deviations for rings with $n \geq 10$ would be relatively insignificant. Although one may attempt to correlate the overall blue shift of the Raman band in the bending vibration region with the shift of the ring size distribution to larger rings, we could not see any reason that those two trends must be coupled or correlated at this moment.

4. Conclusions

IR and Raman spectroscopy analyses for silica and a series of sodium silicate glasses $[\text{Na}_2\text{O}]_x[\text{Al}_2\text{O}_3]_2[\text{SiO}_2]_{98-x}$ with $x = 7, 12, 17,$ and 22 were performed and various possible correlations between vibrational spectral features and structural parameters of the silicate glass network were tested. To obtain the structural parameters appropriate for comparison with the experimental data, MD simulations were carried out using three types of potentials: partial charge pairwise potential (Teter), partial diffuse charge potential (MGFF), and bond order based potential with charge transfer effect (ReaxFF force fields). Among these three potentials, ReaxFF-MD simulations produced theoretical IR spectra that resemble most the experimental data in terms of peak position and relative peak intensity. The comparison of experimentally observed spectral changes as a function of the sodium modifier ion concentration and the structural parameters obtained from ReaxFF-MD simulation were made and the results raised serious questions about the adequacy or validity of previously used spectral interpretation schemes. The asymmetric Si-O stretch band position in IR does not correlate well with the Si-O-

Si bond angle; instead, it correlates linearly with the Si-O bond length change. The Si-O stretch band in Raman cannot be deconvoluted with the Q^n speciation; instead, it might be related to activation of structurally-restricted stretching vibrational modes of randomly-connected SiO_4 units upon reduction of the network connectivity with increasing the network modifier concentration. The relative intensities of the Si-O-Si bending vibration bands in Raman cannot be explained by changes in the $(SiO)_n$ ring size distribution of the silicate network. Instead, they may reflect the changes in the bond length and angle of the dominant rings with $n = 5\sim 9$. The results of this study thus raise serious concerns or questions on the adequacy of the widely-cited and used peak assignment and interpretation schemes based on molecular or cluster models and, based on these results, we propose alternative approaches for the peak assignments and understanding the composition dependence of the IR and Raman peaks. These assignment and interpretation still need further confirmation in wider ranges of glass compositions.

Acknowledgements. This work was supported by the National Science Foundation (Grant No. DMR-1609170). The Teter and MGFF calculation parts were supported as part of the Center for Performance and Design of Nuclear Waste Forms and Containers, an Energy Frontier Research Center funded by the U.S. Department of Energy, Office of Science, Basic Energy Sciences under Award # DE-SC0016584. HL received the support from the Corning STEM Fellowship program. The authors acknowledge Jingshi Wu for glass sample assistance and SEM image assistance, and acknowledge Huseyin Kaya and Dien Ngo for helpful discussion.

References

1. Varshneya AK. Fundamentals of inorganic glasses: Elsevier; 2013.
2. Soules T. A molecular dynamic calculation of the structure of sodium silicate glasses. *The Journal of Chemical Physics*. 1979;71(11):4570-8.
3. Meyer A, Horbach J, Kob W, Kargl F, Schober H. Channel formation and intermediate range order in sodium silicate melts and glasses. *Physical Review Letters*. 2004;93(2):027801.
4. Huang C, Cormack A. The structure of sodium silicate glass. *The Journal of chemical physics*. 1990;93(11):8180-6.
5. Horbach J, Kob W, Binder K. Dynamics of sodium in sodium disilicate: channel relaxation and sodium diffusion. *Physical review letters*. 2002;88(12):125502.
6. Dell W, Bray P, Xiao S. ¹¹B NMR studies and structural modeling of Na₂O-B₂O₃-SiO₂ glasses of high soda content. *Journal of Non-Crystalline Solids*. 1983;58(1):1-16.
7. Du L-S, Stebbins JF. Network connectivity in aluminoborosilicate glasses: A high-resolution ¹¹B, ²⁷Al and ¹⁷O NMR study. *Journal of Non-Crystalline Solids*. 2005;351(43-45):3508-20.
8. Wright AC. Neutron scattering from vitreous silica. V. The structure of vitreous silica: What have we learned from 60 years of diffraction studies? *Journal of non-crystalline solids*. 1994;179:84-115.
9. Gaskell P. Vibrational spectra of simple silicate glasses. *Discussions of the Faraday Society*. 1970;50:82-93.
10. McMillan P. Structural studies of silicate glasses and melts—applications and limitations of Raman spectroscopy. *American Mineralogist*. 1984;69(7-8):622-44.
11. Hanna R, Su GJ. Infrared Absorption Spectra of Sodium Silicate Glasses from 4 to 30- μ . *Journal of the American Ceramic Society*. 1964;47(12):597-601.
12. Sweet JR, White WB. Infrared Reflectance Spectrometer for Liquids at High Temperatures. *Appl Spectrosc*. 1969;23(3):230-&.
13. Crozier D, Douglas R. Study of sodium silicate glasses in infra-red by means of thin films. *Phys Chem Glasses*. 1965;6(6):240-&.
14. Husung RD, Doremus RH. The infrared transmission spectra of four silicate glasses before and after exposure to water. *Journal of Materials Research*. 1990;5(10):2209-17.
15. Amma S, Luo JW, Pantano CG, Kim SH. Specular reflectance (SR) and attenuated total reflectance (ATR) infrared (IR) spectroscopy of transparent flat glass surfaces: A case study for soda lime float glass. *Journal of Non-Crystalline Solids*. 2015;428:189-96.
16. Almeida RM, Pantano CG. Structural investigation of silica gel films by infrared spectroscopy. *J Appl Phys*. 1990;68(8):4225-32.
17. Bell R, Dean P, Hibbins-Butler D. Normal mode assignments in vitreous silica, germania and beryllium fluoride. *Journal of Physics C: Solid State Physics*. 1971;4(10):1214.
18. Scott J, Porto S. Longitudinal and transverse optical lattice vibrations in quartz. *Phys Rev*. 1967;161(3):903.
19. Bates JB. Raman spectra of α and β cristobalite. *The Journal of Chemical Physics*. 1972;57(9):4042-7.
20. Laughlin R, Joannopoulos J. Phonons in amorphous silica. *Physical Review B*. 1977;16(6):2942.
21. Brawer S. Theory of the vibrational spectra of some network and molecular glasses. *Physical Review B*. 1975;11(8):3173.
22. Furukawa T, Fox KE, White WB. Raman spectroscopic investigation of the structure of silicate glasses. III. Raman intensities and structural units in sodium silicate glasses. *The Journal of Chemical Physics*. 1981;75(7):3226-37.
23. Sanders D, Person W, Hench L. Quantitative analysis of glass structure with the use of infrared reflection spectra. *Appl Spectrosc*. 1974;28(3):247-55.

24. Luo J, Smith NJ, Pantano CG, Kim SH. Complex refractive index of silica, silicate, borosilicate, and borosiluminosilicate glasses—Analysis of glass network vibration modes with specular-reflection IR spectroscopy. *Journal of Non-Crystalline Solids*. 2018;494:94-103.
25. De Aza P, Santos C, Pazo A, De Aza S, Cusco R, Artus L. Vibrational properties of calcium phosphate compounds. 1. Raman spectrum of β -tricalcium phosphate. *Chemistry of materials*. 1997;9(4):912-5.
26. Mihailova B, Bismayer U, Engelhardt A, Güttler B. Wall-related Raman scattering in ferroelastic lead phosphate $Pb_3(PO_4)_2$. *Journal of Physics: Condensed Matter*. 2001;13(41):9383.
27. Hamilton VE. Thermal infrared (vibrational) spectroscopy of Mg–Fe olivines: A review and applications to determining the composition of planetary surfaces. *Chemie der Erde-Geochemistry*. 2010;70(1):7-33.
28. Tuschel D. Why are the Raman spectra of crystalline and amorphous solids different? 2017.
29. Smith Jr J, Brodsky M, Crowder B, Nathan M, Pinczuk A. Raman spectra of amorphous Si and related tetrahedrally bonded semiconductors. *Physical Review Letters*. 1971;26(11):642.
30. Sen P, Thorpe M. Phonons in A X 2 glasses: from molecular to band-like modes. *Physical Review B*. 1977;15(8):4030.
31. Agarwal A, Tomozawa M. Correlation of silica glass properties with the infrared spectra. *Journal of Non-Crystalline Solids*. 1997;209(1-2):166-74.
32. Ishikawa K, Suzuki K, Okamura S. Asymmetric peak line shape of infrared dielectric function spectra for thermally grown silicon dioxide films. *J Appl Phys*. 2000;88(12):7150-6.
33. Galeener FL. Band limits and the vibrational spectra of tetrahedral glasses. *Physical Review B*. 1979;19(8):4292.
34. Luo J, Zhou Y, Milner ST, Pantano CG, Kim SH. Molecular dynamics study of correlations between IR peak position and bond parameters of silica and silicate glasses: Effects of temperature and stress. *Journal of the American Ceramic Society*. 2018;101(1):178-88.
35. Luo J, Zhou Y, Pantano CG, Kim SH. Correlation between IR peak position and bond parameter of silica glass: Molecular dynamics study on fictive temperature (cooling rate) effect. *Journal of the American Ceramic Society*. 2018;101(12):5419-27.
36. Brawer SA, White WB. Raman spectroscopic investigation of the structure of silicate glasses. I. The binary alkali silicates. *The Journal of Chemical Physics*. 1975;63(6):2421-32.
37. Sharma SK, Mammone JF, Nicol MF. Raman investigation of ring configurations in vitreous silica. *Nature*. 1981;292(5819):140.
38. Galeener FL. Planar rings in vitreous silica. *Journal of Non-Crystalline Solids*. 1982;49(1-3):53-62.
39. Sykes D, Kubicki J. Four-membered rings in silica and aluminosilicate glasses. *Mineralogical Society of America*; 1996.
40. Kubicki J, Sykes D. Molecular orbital calculations of vibrations in three-membered aluminosilicate rings. *Physics and Chemistry of Minerals*. 1993;19(6):381-91.
41. Hunt JD, Kavner A, Schauble EA, Snyder D, Manning CE. Polymerization of aqueous silica in H_2O – K_2O solutions at 25–200 C and 1 bar to 20 kbar. *Chemical Geology*. 2011;283(3-4):161-70.
42. Spiekermann G, Steele-MacInnis M, Kowalski PM, Schmidt C, Jahn S. Vibrational mode frequencies of H_4SiO_4 , D_4SiO_4 , $H_6Si_2O_7$, and $H_6Si_3O_9$ in aqueous environment, obtained from ab initio molecular dynamics. *The Journal of chemical physics*. 2012;137(16):164506.
43. Uchino T, Iwasaki M, Sakka T, Ogata Y. Ab initio molecular orbital calculations on the electronic structure of sodium silicate glasses. *The Journal of Physical Chemistry*. 1991;95(14):5455-62.
44. Simon I, McMahon HO. Study of Some Binary Silicate Glasses by Means of Reflection in Infrared. *Journal of the American Ceramic Society*. 1953;36(5):160-4.

45. Corrales LR, Du J. Characterization of ion distributions near the surface of sodium - containing and sodium - depleted calcium aluminosilicate melts. *Journal of the American Ceramic Society*. 2006;89(1):36-41.
46. Du J, Cormack AN. Molecular dynamics simulation of the structure and hydroxylation of silica glass surfaces. *Journal of the American Ceramic Society*. 2005;88(9):2532-9.
47. Hahn SH, Rimsza J, Criscenti L, Sun W, Deng L, Du J, et al. Development of a ReaxFF Reactive Force Field for NaSiO_x/Water Systems and Its Application to Sodium and Proton Self-Diffusion. *The Journal of Physical Chemistry C*. 2018;122(34):19613-24.
48. Mahadevan T, Garofalini S. Dissociative chemisorption of water onto silica surfaces and formation of hydronium ions. *The Journal of Physical Chemistry C*. 2008;112(5):1507-15.
49. Mahadevan TS, Du J. Evaluating Water Reactivity at Silica Surfaces Using Reactive Potentials. *The Journal of Physical Chemistry C*. 2018;122(18):9875-85.
50. Simmons JH, Mohr RK, Montrose C. Non - Newtonian viscous flow in glass. *J Appl Phys*. 1982;53(6):4075-80.
51. Wu J, Cai L. Phase separation in Li- and Na- silicate glasses. American Ceramic Society- Glass and Optical Materials Division Meeting. 2018;San Antonio, Texas.
52. Yamamoto Y, Yamamoto K. Precise XPS depth profile of soda-lime-silica float glass using C-60 ion beam. *Opt Mater*. 2011;33(12):1927-30.
53. Wassick T, Doremus R, Lanford W, Burman C. Hydration of soda-lime silicate glass, effect of alumina. *Journal of non-crystalline solids*. 1983;54(1-2):139-51.
54. Du J, Cormack A. The medium range structure of sodium silicate glasses: a molecular dynamics simulation. *Journal of Non-Crystalline Solids*. 2004;349:66-79.
55. Mahadevan TS, Sun W, Du J. Development of Water Reactive Potentials for Sodium Silicate Glasses. *The Journal of Physical Chemistry B*. 2019.
56. Van Duin AC, Dasgupta S, Lorant F, Goddard WA. ReaxFF: a reactive force field for hydrocarbons. *The Journal of Physical Chemistry A*. 2001;105(41):9396-409.
57. Senftle TP, Hong S, Islam MM, Kylasa SB, Zheng Y, Shin YK, et al. The ReaxFF reactive force-field: development, applications and future directions. *npj Computational Materials*. 2016;2:15011.
58. Liang T, Shin YK, Cheng Y-T, Yilmaz DE, Vishnu KG, Veners O, et al. Reactive potentials for advanced atomistic simulations. *Annual review of materials research*. 2013;43:109-29.
59. Plimpton S. Fast parallel algorithms for short-range molecular dynamics. *Journal of computational physics*. 1995;117(1):1-19.
60. Pitman MC, Van Duin AC. Dynamics of confined reactive water in smectite clay–zeolite composites. *Journal of the American Chemical Society*. 2012;134(6):3042-53.
61. Doremus RH. Infrared spectroscopy of surfaces of glasses containing alkali ions. *Journal of Non Crystalline Solids*. 1980;41:145-9.
62. Simon I. Infrared studies of glass. *Modern aspects of the vitreous state*. 1960;1:120-51.
63. Yamamoto K, Ishida H. Kramers-Kronig analysis applied to reflection-absorption spectroscopy. *Vibrational spectroscopy*. 1997;15(1):27-36.
64. Jellyman P, Procter J. Infrared reflection spectra of glasses. *J Soc Glass Technol*. 1955;39:173-92T.
65. Kirk C. Quantitative analysis of the effect of disorder-induced mode coupling on infrared absorption in silica. *Physical Review B*. 1988;38(2):1255.
66. Liu H, Ngo D, Ren M, Du J, Kim SH. Effects of surface initial condition on aqueous corrosion of glass—A study with a model nuclear waste glass. *Journal of the American Ceramic Society*. 2019;102(4):1652-64.
67. Galeener F, Lucovsky G. Longitudinal Optical Vibrations in Glasses: Ge O₂ and Si O₂. *Physical Review Letters*. 1976;37(22):1474.

68. Gunde MK. Vibrational modes in amorphous silicon dioxide. *Physica B: Condensed Matter*. 2000;292(3-4):286-95.
69. Wilson EB, Decius JC, Cross PC. *Molecular vibrations: the theory of infrared and Raman vibrational spectra*: Courier Corporation; 1980.
70. Herzbach D, Binder K, Müser MH. Comparison of model potentials for molecular-dynamics simulations of silica. *The Journal of chemical physics*. 2005;123(12):124711.
71. Yuan X, Cormack AN. Local structures of MD-modeled vitreous silica and sodium silicate glasses. *Journal of non-crystalline solids*. 2001;283(1-3):69-87.
72. Zhang W, Chen X, Van Duin AC. Isotope effects in water: Differences of structure, dynamics, spectrum, and proton transport between heavy and light water from ReaxFF reactive force field simulations. *The journal of physical chemistry letters*. 2018;9(18):5445-52.
73. Xiang Y, Du J, Skinner LB, Benmore CJ, Wren AW, Boyd DJ, et al. Structure and diffusion of ZnO–SrO–CaO–Na₂O–SiO₂ bioactive glasses: a combined high energy X-ray diffraction and molecular dynamics simulations study. *RSC Advances*. 2013;3(17):5966.
74. Ren M, Du J. Structural origin of the thermal and diffusion behaviors of lithium aluminosilicate crystal polymorphs and glasses. *Journal of the American Ceramic Society*. 2016;99(8):2823-33.
75. Ren M, Cheng JY, Jaccani SP, Kapoor S, Youngman RE, Huang L, et al. Composition–structure–property relationships in alkali aluminosilicate glasses: A combined experimental–computational approach towards designing functional glasses. *Journal of Non-Crystalline Solids*. 2019;505:144-53.
76. Deng L, Urata S, Takimoto Y, Miyajima T, Hahn SH, van Duin AC, et al. Structural features of sodium silicate glasses from Reactive Force Field based molecular dynamics simulations. *Journal of the American Ceramic Society*.
77. Hemmati M, Angell CA. IR absorption of silicate glasses studied by ion dynamics computer simulation. I. IR spectra of SiO₂ glass in the rigid ion model approximation. *Journal of non-crystalline solids*. 1997;217(2-3):236-49.
78. Galeener F. Planar rings in glasses. *Solid State Communications*. 1982;44(7):1037-40.
79. Devine R. Ion implantation-and radiation-induced structural modifications in amorphous SiO₂. *Journal of non-crystalline solids*. 1993;152(1):50-8.
80. Wright AC, Clare AG, Bachra B, Sinclair RN, Hannon AC, Vessal B. Neutron diffraction studies of silicate glasses. *Trans Am Crystallogr Assoc*. 1991;27(1):239-54.
81. Yuan X, Cormack A. Si–O–Si bond angle and torsion angle distribution in vitreous silica and sodium silicate glasses. *Journal of non-crystalline solids*. 2003;319(1-2):31-43.
82. Berreman DW. Kramers-Kronig analysis of reflectance measured at oblique incidence. *Applied optics*. 1967;6(9):1519-21.
83. Lindon JC, Tranter GE, Koppelaar D. *Encyclopedia of spectroscopy and spectrometry*: Academic Press; 2016.
84. Knapp E, Fischer S. On the theory of homogeneous and inhomogeneous line broadening. An exactly solvable model. *The Journal of Chemical Physics*. 1981;74(1):89-95.
85. Oxtoby DW. Dephasing of molecular vibrations in liquids. *Advances in Chemical Physics*. 1979:1-48.
86. Dupree R, Holland D, McMillan PW, Pettifer R. The structure of soda-silica glasses: a MAS NMR study. *Journal of Non-Crystalline Solids*. 1984;68(2-3):399-410.
87. Gross E, Kolesova V. Raman spectra and structure of glassy substances. *The structure of glass*. 1958;1:45.
88. Bobovich YS, Tulub T. Raman spectra and structure of certain silicate glasses. *The Structure of Glass*. 1959;2:173-6.
89. Yadav AK, Singh P. A review of the structures of oxide glasses by Raman spectroscopy. *Rsc Advances*. 2015;5(83):67583-609.

90. Maekawa H, Maekawa T, Kawamura K, Yokokawa T. The structural groups of alkali silicate glasses determined from ^{29}Si MAS-NMR. *Journal of Non-Crystalline Solids*. 1991;127(1):53-64.
91. Shuker R, Gammon RW. Raman-scattering selection-rule breaking and the density of states in amorphous materials. *Physical Review Letters*. 1970;25(4):222.
92. Lehmann A, Schumann L, Hübner K. Optical Phonons in Amorphous Silicon Oxides. I. Calculation of the Density of States and Interpretation of Lo-To Splittings of Amorphous SiO_2 . *Physica status solidi (b)*. 1983;117(2):689-98.
93. Krishnan R. Raman spectrum of quartz. *Nature*. 1945;155(3937):452.
94. Ferrari AC. Raman spectroscopy of graphene and graphite: disorder, electron–phonon coupling, doping and nonadiabatic effects. *Solid state communications*. 2007;143(1-2):47-57.
95. Campos-Delgado J, Kim Y, Hayashi T, Morelos-Gómez A, Hofmann M, Muramatsu H, et al. Thermal stability studies of CVD-grown graphene nanoribbons: Defect annealing and loop formation. *Chemical Physics Letters*. 2009;469(1-3):177-82.

List of Table Captions

Table 1. Composition determined with XRF and density measured with buoyance method for a series of sodium silicates $[\text{Na}_2\text{O}]_x[\text{Al}_2\text{O}_3]_2[\text{SiO}_2]_{98-x}$ with $X=7, 12, 17, 22$.

Table 2. Oxygen speciation (atom-%) obtained from ReaxFF-MD simulations for a series of sodium silicate glasses with the same compositions of the experimental samples.

List of Figure Captions

Figure 1. (a) Specular-reflectance IR spectra, and (b) Raman spectra for a series of sodium silicate glasses $[\text{Na}_2\text{O}]_x[\text{Al}_2\text{O}_3]_2[\text{SiO}_2]_{98-x}$ with $X=7, 12, 17, 22$. For comparison, the IR and Raman spectra of silica (modeled with fused quartz) and z-cut crystalline quartz are also shown.

Figure 2. Comparison of IR spectra calculated from MD simulations using (a) Teter, (b) MGFF, and (c) ReaxFF force field for a series of sodium silicate glasses $[\text{Na}_2\text{O}]_x[\text{Al}_2\text{O}_3]_2[\text{SiO}_2]_{98-x}$ with $X=7, 12, 17, 22$.

Figure 3. IR spectra calculated for (a) BO only and (b) NBO only by MD with ReaxFF force fields for a series of sodium silicate glasses $[\text{Na}_2\text{O}]_x[\text{Al}_2\text{O}_3]_2[\text{SiO}_2]_{98-x}$ with $X=7, 12, 17, 22$.

Figure 4. Distributions of (a) Si-BO bond length with inset of FWHM of Si-BO, (b) Si-NBO bond length with inset of FWHM of Si-NBO, and (c) Si-O-Si bond angle obtained from ReaxFF-MD simulations of a series of sodium silicate glasses $[\text{Na}_2\text{O}]_x[\text{Al}_2\text{O}_3]_2[\text{SiO}_2]_{98-x}$ with $X=7, 12, 17, 22$.

Figure 5. Correlation between the mean value of the experimentally measured stretch band (Figure 1a) and the weighted averages of (a) all Si-O bond length distribution, (b) Si-BO bond length distribution, and (c) Si-O-Si bond angle distribution.

Figure 6. Q_n speciation simulated by ReaxFF-MD for a series of sodium silicate glasses $[\text{Na}_2\text{O}]_x[\text{Al}_2\text{O}_3]_2[\text{SiO}_2]_{98-x}$ with $X=7, 12, 17, 22$.

Figure 7. (a) Ring size distribution for a series of sodium silicate glasses $[\text{Na}_2\text{O}]_x[\text{Al}_2\text{O}_3]_2[\text{SiO}_2]_{98-x}$ with $X=7, 12, 17, 22$ by ReaxFF-MD. Also shown are examples of (b) 3-membered, (c) 6-membered, and (d) 10-membered rings in the glass (snapshots from MD).

Figure 8. Relationship between (a) Si-O bond length and ring size, as well as (b) Si-O-Si bond angle and ring size for a series of sodium silicate glasses $[\text{Na}_2\text{O}]_x[\text{Al}_2\text{O}_3]_2[\text{SiO}_2]_{98-x}$ with $X=7, 12, 17, 22$ by ReaxFF-MD.

Tables

Table 1. Composition determined with XRF and density measured with buoyance method for a series of sodium silicates $[\text{Na}_2\text{O}]_x[\text{Al}_2\text{O}_3]_2[\text{SiO}_2]_{98-x}$ with $X=7, 12, 17, 22$.

Glass composition	Na_2O (mol. %)	Al_2O_3 (mol. %)	SiO_2 (mol. %)	Density ₃ (g/cm ³)
$[\text{Na}_2\text{O}]_7[\text{Al}_2\text{O}_3]_2[\text{SiO}_2]_{91}$	6.9	2.0	91.1	2.277
$[\text{Na}_2\text{O}]_{12}[\text{Al}_2\text{O}_3]_2[\text{SiO}_2]_{86}$	11.6	2.0	86.4	2.327
$[\text{Na}_2\text{O}]_{17}[\text{Al}_2\text{O}_3]_2[\text{SiO}_2]_{81}$	16.4	2.0	81.6	2.372
$[\text{Na}_2\text{O}]_{22}[\text{Al}_2\text{O}_3]_2[\text{SiO}_2]_{76}$	21.3	2.0	76.7	2.418

Table 2. Oxygen speciation (atom-%) obtained from ReaxFF-MD simulations for a series of sodium silicate glasses with the same compositions of the experimental samples.

	Si-BO	Si-NBO	Si-O-Al
7% Na ₂ O	86.6	5.1	8.1
12% Na ₂ O	81.0	10.4	8.6
17% Na ₂ O	75.2	15.9	8.7
22% Na ₂ O	69.2	21.9	8.7

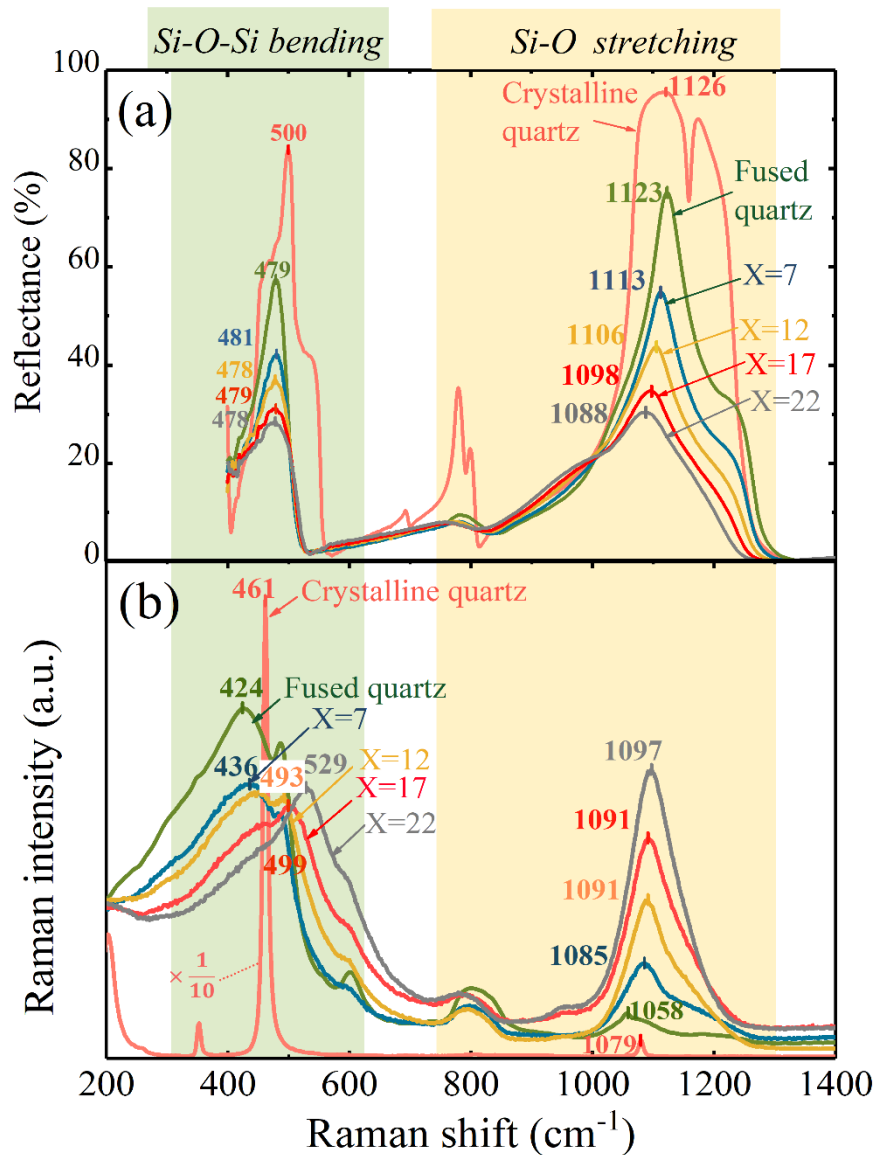


Figure 1. (a) Specular-reflectance IR spectra, and (b) Raman spectra for a series of sodium silicate glasses $[\text{Na}_2\text{O}]_x[\text{Al}_2\text{O}_3]_2[\text{SiO}_2]_{98-x}$ with $X=7, 12, 17, 22$. For comparison, the IR and Raman spectra of silica (modeled with fused quartz) and z-cut crystalline quartz are also shown.

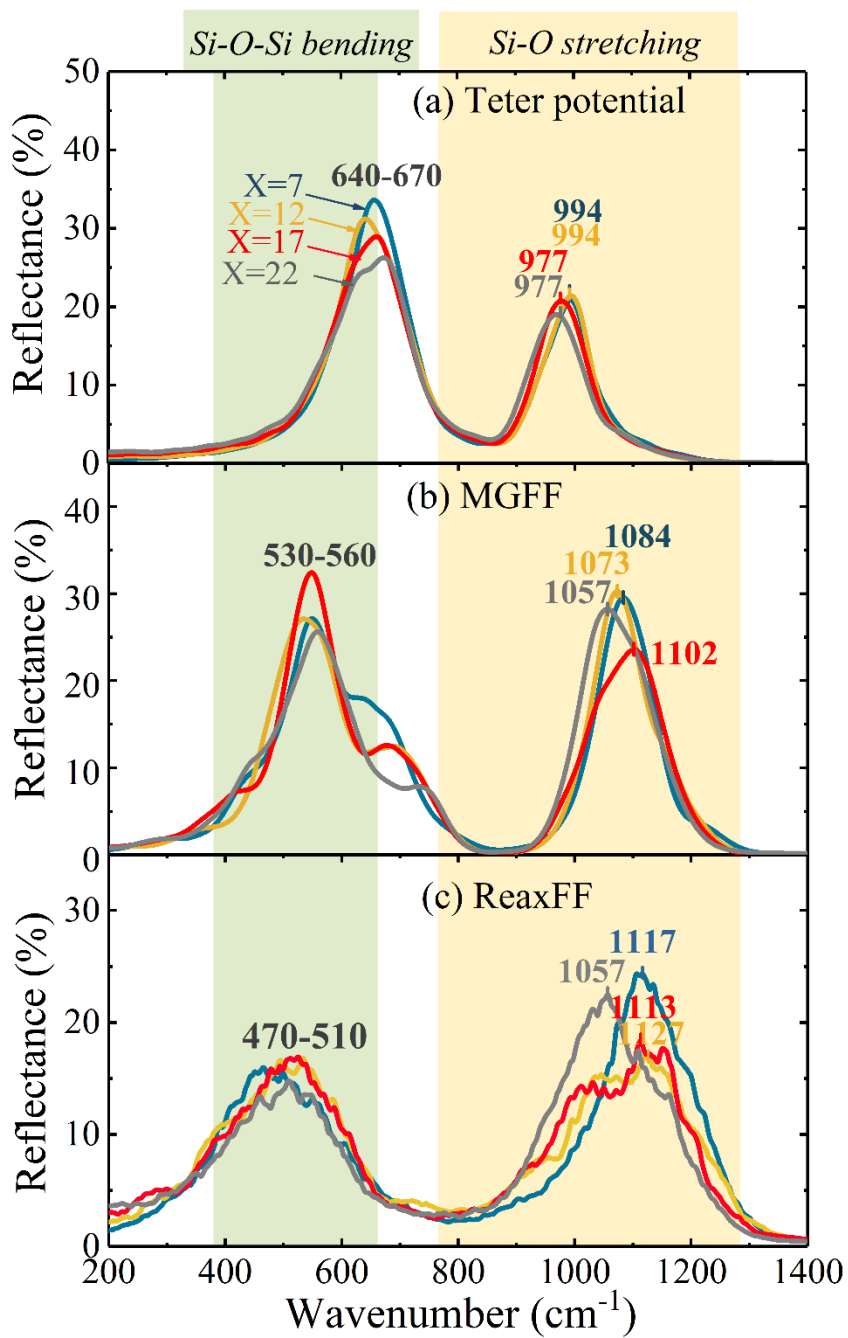


Figure 2. Comparison of IR spectra calculated from MD simulations using (a) Teter, (b) MGFF, and (c) ReaxFF force field for a series of sodium silicate glasses $[\text{Na}_2\text{O}]_x[\text{Al}_2\text{O}_3]_2[\text{SiO}_2]_{98-x}$ with $X=7, 12, 17, 22$.

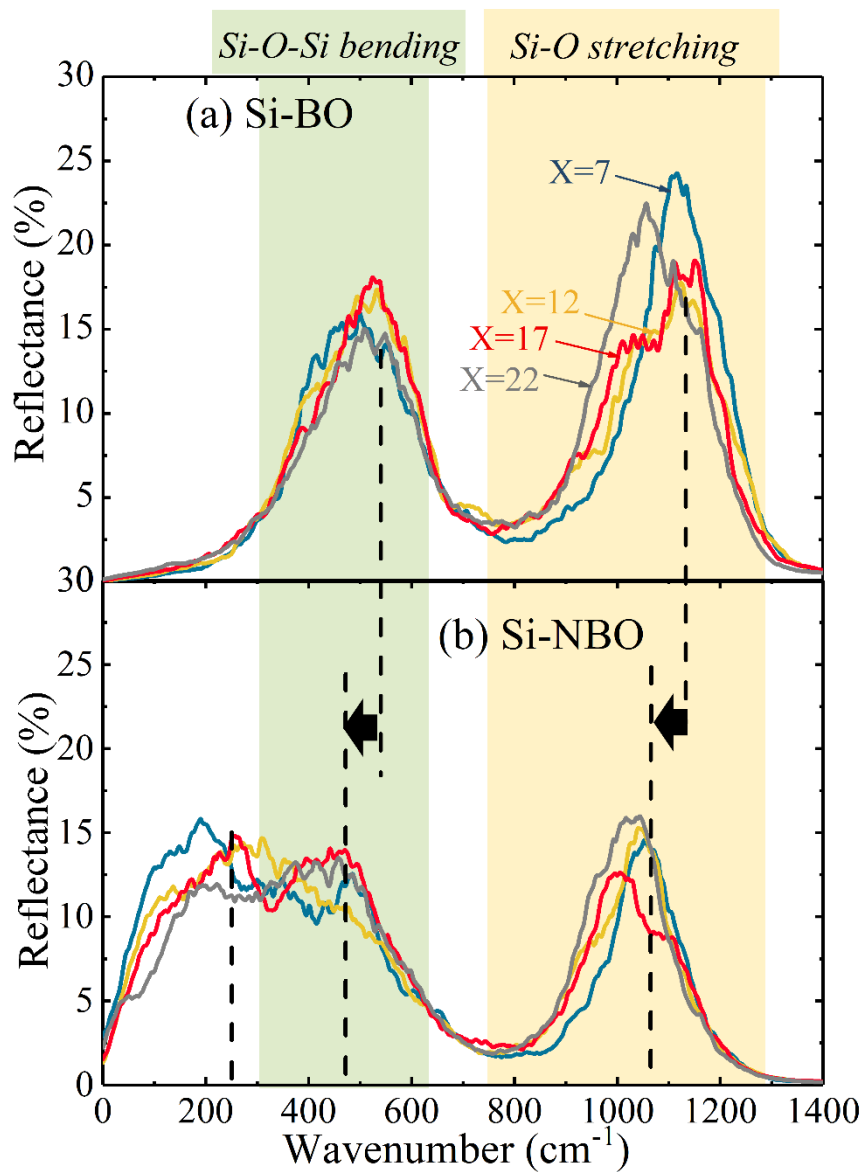


Figure 3. IR spectra calculated for (a) BO only and (b) NBO only by MD with ReaxFF force fields for a series of sodium silicate glasses $[\text{Na}_2\text{O}]_x[\text{Al}_2\text{O}_3]_2[\text{SiO}_2]_{98-x}$ with $X=7, 12, 17, 22$.

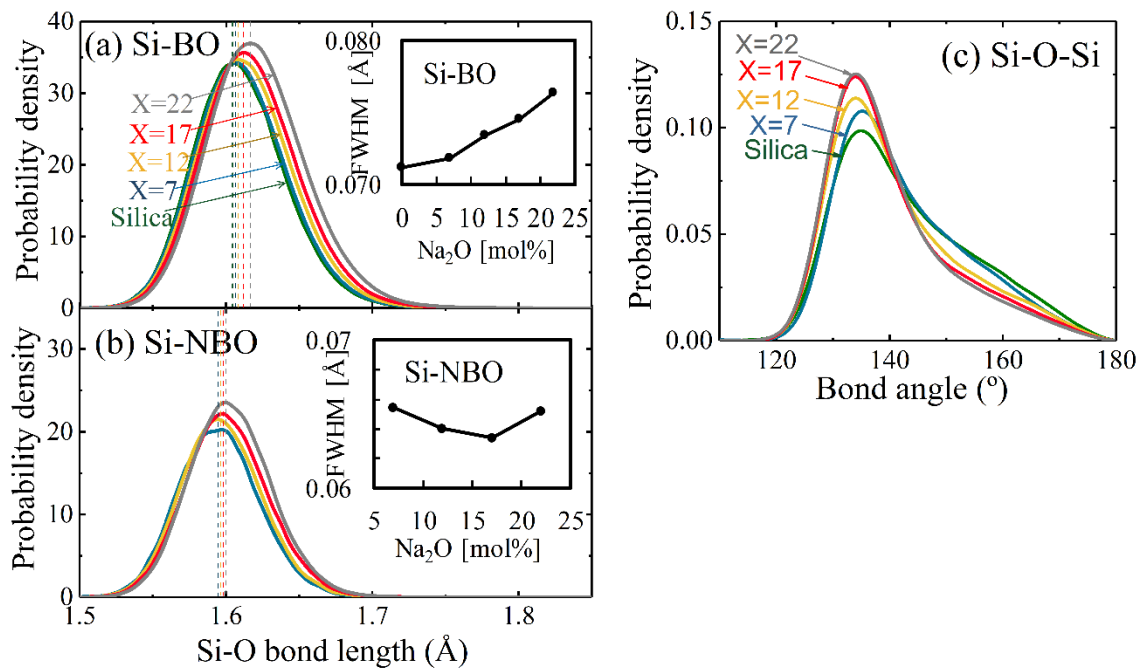


Figure 4. Distributions of (a) Si-BO bond length with inset of FWHM of Si-BO, (b) Si-NBO bond length with inset of FWHM of Si-NBO, and (c) Si-O-Si bond angle obtained from ReaxFF-MD simulations of a series of sodium silicate glasses $[\text{Na}_2\text{O}]_x[\text{Al}_2\text{O}_3]_2[\text{SiO}_2]_{98-x}$ with $X=7, 12, 17, 22$.

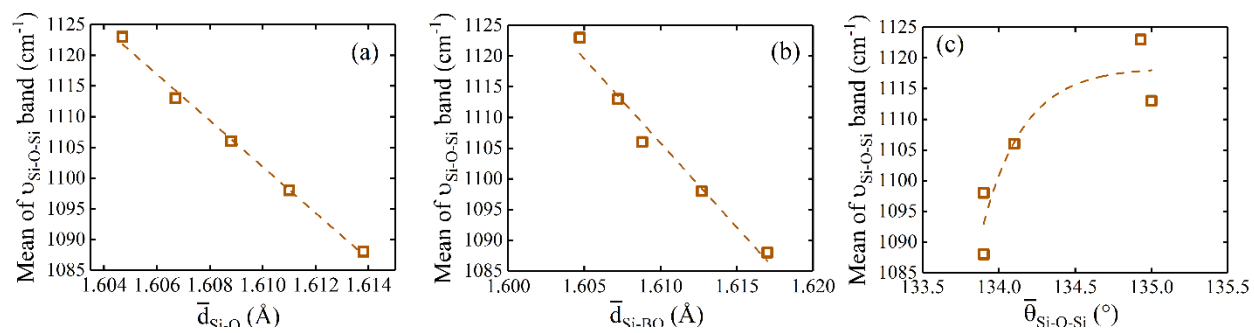


Figure 5. Correlation between the mean value of the experimentally measured stretch band (Figure 1a) and the weighted averages of (a) all Si-O bond length distribution, (b) Si-BO bond length distribution, and (c) Si-O-Si bond angle distribution.

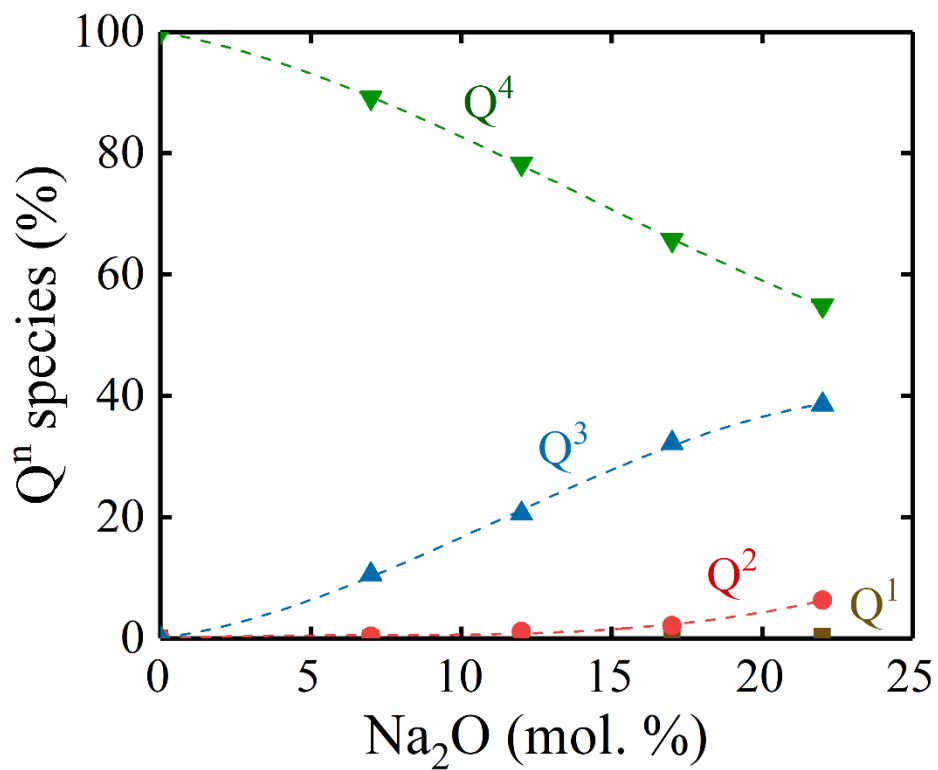


Figure 6. Q_n speciation simulated by ReaxFF-MD for a series of sodium silicate glasses [Na₂O]_x[Al₂O₃]₂[SiO₂]_{98-x} with X=7, 12, 17, 22.

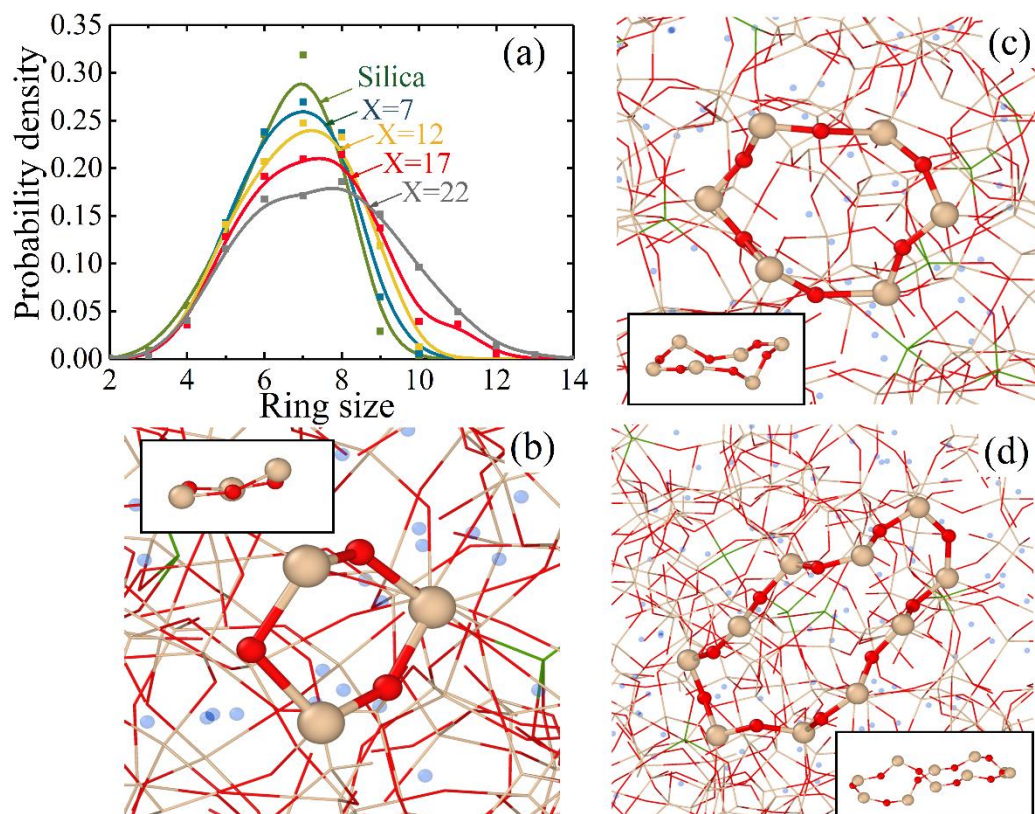


Figure 7. (a) Ring size distribution for a series of sodium silicate glasses $[\text{Na}_2\text{O}]_x[\text{Al}_2\text{O}_3]_2[\text{SiO}_2]_{98-x}$ with $X=7, 12, 17, 22$ by ReaxFF-MD. Also shown are examples of (b) 3-membered, (c) 6-membered, and (d) 10-membered rings in the glass (snapshots from MD).

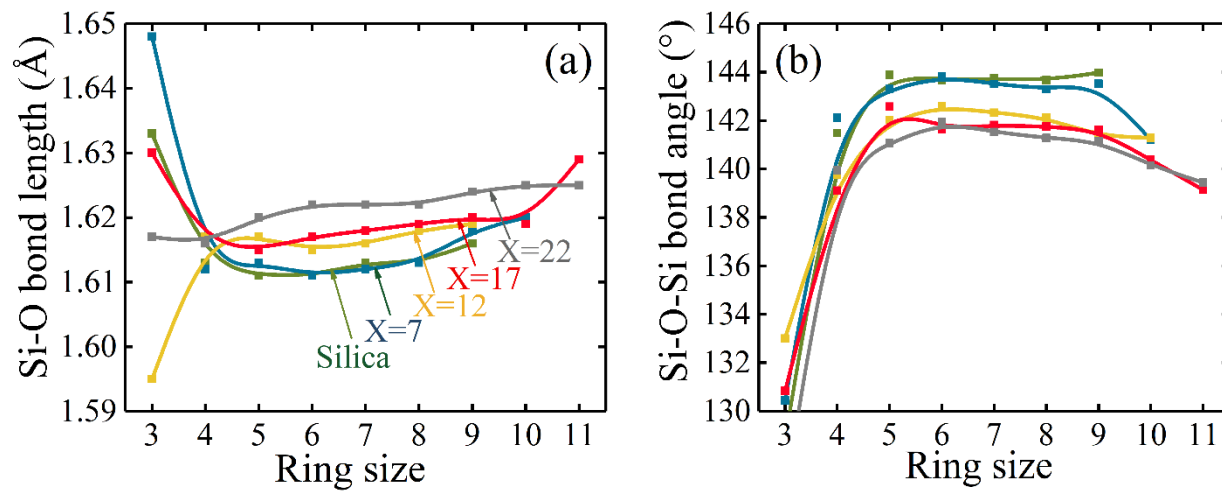


Figure 8. Relationship between (a) Si-O bond length and ring size, as well as (b) Si-O-Si bond angle and ring size for a series of sodium silicate glasses $[\text{Na}_2\text{O}]_x[\text{Al}_2\text{O}_3]_2[\text{SiO}_2]_{98-x}$ with $X=7, 12, 17, 22$ by ReaxFF-MD.

Supporting information

Searching for correlations between vibrational spectral features and structural parameters of silicate glass network

Hongshen Liu,^{a+} Seung Ho Hahn,^{b+} Mengguo Ren,^c Mahadevan Thiruvillamalai,^c Timothy M.
Gross,^d Jincheng Du,^c Adri C. T. van Duin,^{a,b} and Seong H. Kim^{a,*}

^a Department of Chemical Engineering and Materials Research Institute, The Pennsylvania
State University, University Park, PA 16802, USA

^b Department of Mechanical Engineering, The Pennsylvania State University, University Park,
PA 16802, USA

^c Department of Material Science and Engineering, University of North Texas, Denton, TX
76203, USA

^d Corning Research and Development Corporation, Corning, NY 14831, USA

⁺ equal contributions

*Corresponding author: shk10@psu.edu

MD simulation details for glass preparation and IR spectra production

For the structural analysis and IR spectra prediction with the computational methods, $[\text{Na}_2\text{O}]_x[\text{Al}_2\text{O}_3]_2[\text{SiO}_2]_{98-x}$ ($X=7, 12, 17, 22$) sodium silicate glass was modeled in the following way. Total of 3040 particles were first randomly inserted into a cubic simulation box that corresponds to the initial density value given in Table S1. The initial configuration was minimized with conjugate gradient style to avoid any unphysical contact prior to melting the system at high temperatures. Each glass system was then equilibrated at 4000 K for 0.5 ns, followed by gradual cooling at a rate of 0.5 K/ps. Once the system had reached 300K, it was equilibrated for another 0.5 ns. All of the equilibration had been simulated with the NVT (constant number of atoms, volume and temperature) ensemble. This was to keep the system density consistent throughout the glass construction process with Teter potential prior to adopting ReaxFF potential for production (data-gathering) runs. The cooling rate employed in MD simulations is several orders of magnitude higher than that in experiments. However, it is known that the cooling rate effect on glass structure is not substantial if the rate is below 0.2-10 K/ps in MD.^{1, 2, 3, 4} As mentioned in the main text, we constructed the glass system using Teter potential for sodium silicate glasses to reduce the computational cost while ensuring the reproducibility in structural features of our system of interest.

After substituting the potential to ReaxFF, each system with different composition was energy-minimized and then equilibrated under NPT ensemble (constant number of atoms, pressure and temperature) for 200 ps at 300 K, 1 atm. This allows the adaption of the replaced potential to produce the glass structural properties. Finally, 100 ps-long NVT equilibration at 300K was applied to collect the total dipole moment of the system. The glass preparation procedures mentioned above were carried out with the LAMMPS package.⁵ For the glass construction process where Teter potential was employed, a short-range cutoff of 0.55 nm was used for the van de

Waals interaction whereas the particle mesh Ewald (PME) method was used for the long-range Coulomb interaction with a real-space cutoff of 1.2 nm. Also, unless otherwise noted, all simulations employed a time step of 1 fs for this rigid ionic potential along with the damping constant of 100 fs for the thermostat in NVT ensemble. For the ReaxFF-MD runs, shorter time step of 0.25 fs was employed to properly observe the charge transfer between adjacent atoms along the trajectory. Damping constants of 100 fs and 0.5 ps were used for thermo and barostat respectively.

Table S1. Initial simulation box configuration for $[\text{Na}_2\text{O}]_x[\text{Al}_2\text{O}_3]_2[\text{SiO}_2]_{98-x}$ ($X=7, 12, 17, 22$) sodium silicate glass preparation

X	Density [g/cm^3]	Box dimension [\AA]	Number of atoms			
			Si	O	Na	Al
7	2.33	35.168	910	1950	140	40
12	2.36	35.037	860	1900	240	40
17	2.39	34.908	810	1850	340	40
22	2.42	34.781	760	1800	440	40

MD simulations of larger systems (6080 atoms) were also conducted with Teter potential and MGFF potential to analyze the IR spectra. For the glass systems with 6080 atoms, a box of side $\sim 43.9\text{\AA}$ was melted and quenched from $\sim 6000\text{K}$ with both potentials to obtain systems of $[\text{Na}_2\text{O}]_x[\text{Al}_2\text{O}_3]_2[\text{SiO}_2]_{98-x}$ ($X=7, 12, 17, 22$) sodium silicate glasses as had been done with the ReaxFF-MD simulations. The resulting systems were run further for 20ps with both the potentials under NVT and NVE conditions while saving at every 1fs step.

Qⁿ speciation calculation for 7% sodium silicate glass by experimentally measured XRF results

Oxygen speciation was calculated by XRF composition with methodology applied in previous publication⁶, the calculated oxygen speciation for 7% Na₂O glass is shown in table S2.

Table S2. Oxygen speciation for 7% sodium silicate glass

	BO	NBO
% (Based on total O)	94.94	5.06

Qⁿ speciation was further calculated by equation (1)-(4).

$$Si_{tot}\% = \frac{(BO\% - NBO\% * 1.5)}{2} + NBO\% \quad (1)$$

$$Si_{NBO}\% = NBO\% \quad (2)$$

$$Q^3\% = \frac{Si_{NBO}\%}{Si_{tot}\%} \quad (3)$$

$$Q^4\% = 100\% - Q^3\% \quad (4)$$

The results were present in table S3.

Table S3. Qⁿ speciation for 7% sodium silicate glass

	Q ⁴ (%)	Q ³ (%)
7% Na ₂ O	89.6	10.4

Si-O-Si angle of different siloxanes

Table S4. Si-O-Si angle of different siloxanes

		$(\text{HO})_3\text{-Si-O-Si-(OH)}_3$	$((\text{CH}_3)_3\text{O})_3\text{-Si-O-Si-(O(CH}_3)_3)_3$
ReaxFF	Na/Si/O/H (2018) ⁷	132.4	144.7
DFT	B3LYP/TZP	127.6	142.2
	B3LYP/6-311G ⁸	143	
	MP2/6-31G* ⁹	123.1	
	HF/6-31G* ⁹	131.8	
	wB97X-D3/def2-TZVP ¹⁰	133.8	

Bond parameters of Al-O in silicate glass network

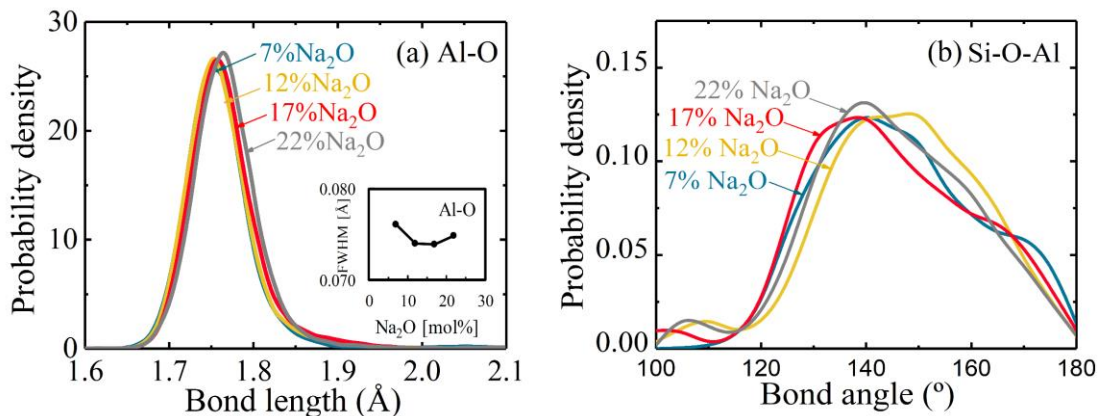


Figure S1. Distributions of (a) Al-O bond length with inset of FWHM of Al-O distribution, and (b) Si-O-Al bond angle obtained from ReaxFF-MD simulations of a series of sodium silicate glasses $[\text{Na}_2\text{O}]_x[\text{Al}_2\text{O}_3]_2[\text{SiO}_2]_{98-x}$ with $X=7, 12, 17, 22$.

ReaxFF Reactive Force Field Parameters for Sodium Aluminosilicate Glass Systems

The force field parameters below can be used with the standalone ReaxFF code, as well as within the LAMMPS open-source MD simulation code and the ReaxFF implementation within the ADF package.

Reactive MD-force field: Si/Al/O/H/Na; JACS 2012, JPCC 2018

```
39  ! Number of general parameters
50.0000 !Overcoordination parameter
9.5469 !Overcoordination parameter
1.6725 !Valency angle conjugation parameter
1.7224 !Triple bond stabilisation parameter
6.8702 !Triple bond stabilisation parameter
60.4850 !C2-correction
1.0588 !Undercoordination parameter
4.6000 !Triple bond stabilisation parameter
12.1176 !Undercoordination parameter
13.3056 !Undercoordination parameter
-40.0000 !Triple bond stabilization energy
0.0000 !Lower Taper-radius
10.0000 !Upper Taper-radius
2.8793 !Not used
33.8667 !Valency undercoordination
6.0891 !Valency angle/lone pair parameter
1.0563 !Valency angle
2.0384 !Valency angle parameter
6.1431 !Not used
6.9290 !Double bond/angle parameter
0.3989 !Double bond/angle parameter: overcoord
3.9954 !Double bond/angle parameter: overcoord
-2.4837 !Not used
5.7796 !Torsion/BO parameter
10.0000 !Torsion overcoordination
1.9487 !Torsion overcoordination
-1.2327 !Conjugation 0 (not used)
2.1645 !Conjugation
1.5591 !vdWaals shielding
0.1000 !Cutoff for bond order (*100)
1.7602 !Valency angle conjugation parameter
0.6991 !Overcoordination parameter
50.0000 !Overcoordination parameter
1.8512 !Valency/lone pair parameter
0.5000 !Not used
20.0000 !Not used
5.0000 !Molecular energy (not used)
0.0000 !Molecular energy (not used)
0.7903 !Valency angle conjugation parameter
7  ! Nr of atoms; cov.r; valency;a.m;Rvdw;Evdw;gammaEEM;cov.r2;#
    alfa;gammavdW;valency;Eunder;Eover;chiEEM;etaEEM;n.u.
    cov r3;Elp;Heat inc.;n.u.;n.u.;n.u.;n.u.
```

```

ov/un;val1;n.u.;val3,vval4
C 1.3817 4.0000 12.0000 1.8903 0.1838 0.6544 1.1341 4.0000
  9.7559 2.1346 4.0000 34.9350 79.5548 5.4088 6.0000 0.0000
  1.2114 0.0000 202.2908 8.9539 34.9289 13.5366 0.8563 0.0000
  -2.8983 2.5000 1.0564 4.0000 2.9663 0.0000 0.0000 0.0000
H 0.8930 1.0000 1.0080 1.3550 0.0930 0.8203 -0.1000 1.0000
  8.2230 33.2894 1.0000 0.0000 121.1250 3.7248 9.6093 1.0000
  -0.1000 0.0000 61.6606 3.0408 2.4197 0.0003 1.0698 0.0000
  -19.4571 4.2733 1.0338 1.0000 2.8793 1.0000 0.2000 12.0000
O 1.2450 2.0000 15.9990 2.3890 0.1000 1.0898 1.0548 6.0000
  9.7300 13.8449 4.0000 37.5000 116.0768 8.5000 8.3122 2.0000
  0.9049 0.4056 59.0626 3.5027 0.7640 0.0021 0.9745 0.0000
  -3.5500 2.9000 1.0493 4.0000 2.9225 1.3000 0.2000 13.0000
Si 2.1932 4.0000 28.0600 1.8951 0.1737 0.8112 1.2962 4.0000
  11.3429 5.2054 4.0000 21.7115 139.9309 4.0081 5.7104 0.0000
  -1.0000 0.0000 128.2031 9.0751 23.8188 0.8381 0.8563 0.0000
  -4.1684 2.0754 1.0338 4.0000 2.5791 1.4000 0.2000 13.0000
Na 1.7878 1.0000 22.9898 2.6441 0.2588 0.8476 -1.0000 1.0000
  9.0003 2.5000 1.0000 0.0000 0.0000 -3.4731 8.1298 0.0000
  -1.0000 0.0000 23.0445 100.0000 1.0000 0.0000 0.8563 0.0000
  -4.1479 3.9900 1.0338 8.0000 2.5791 0.0000 0.0000 0.0000
Al 2.1967 3.0000 26.9820 2.3738 0.2328 0.4558 -1.6836 3.0000
  9.4002 3.9009 3.0000 0.0076 16.5151 1.6032 6.7003 0.0000
  -1.0000 0.0000 78.4675 20.0000 0.2500 0.0000 0.8563 0.0000
  -23.1826 1.5000 1.0338 8.0000 2.5791 1.4000 0.2000 13.0000
X -0.1000 2.0000 1.0080 2.0000 0.0000 1.0000 -0.1000 6.0000
  10.0000 2.5000 4.0000 0.0000 0.0000 8.5000 1.5000 0.0000
  -0.1000 0.0000 127.6226 8.7410 13.3640 0.6690 0.9745 0.0000
  -11.0000 2.7466 1.0338 6.2998 2.8793 0.0000 0.0000 0.0000
20 ! Nr of bonds; Edis1;LPpen;n.u.;pbe1;pbo5;l3corr;pbo6
    pbe2;pbo3;pbo4;n.u.;pbo1;pbo2;ovcorr
1 1 158.2004 99.1897 78.0000 -0.7738 -0.4550 1.0000 37.6117 0.4147
  0.4590 -0.1000 9.1628 1.0000 -0.0777 6.7268 1.0000 0.0000
1 2 169.4760 0.0000 0.0000 -0.6083 0.0000 1.0000 6.0000 0.7652
  5.2290 1.0000 0.0000 1.0000 -0.0553 6.9316 0.0000 0.0000
2 2 153.3934 0.0000 0.0000 -0.4600 0.0000 1.0000 6.0000 0.7300
  6.2500 1.0000 0.0000 1.0000 -0.0790 6.0552 0.0000 0.0000
1 3 100.9167 136.3836 65.3877 0.3895 -0.3906 1.0000 18.8159 0.6674
  1.1202 -0.3411 9.1099 1.0000 -0.1966 5.6975 0.0000 0.0000
3 3 142.2858 145.0000 50.8293 0.2506 -0.1000 1.0000 29.7503 0.6051
  0.3451 -0.1055 9.0000 1.0000 -0.1225 5.5000 1.0000 0.0000
2 3 160.0000 0.0000 0.0000 -0.5725 0.0000 1.0000 6.0000 0.5626
  1.1150 1.0000 0.0000 0.0000 -0.0920 4.2790 0.0000 0.0000
1 4 108.3910 95.0233 0.0000 0.1129 -0.5558 1.0000 17.2117 0.4568
  0.2424 -0.2378 10.1163 1.0000 -0.1020 5.7156 1.0000 0.0000
2 4 250.0000 0.0000 0.0000 -0.7128 0.0000 1.0000 6.0000 0.1186
  18.5790 1.0000 0.0000 1.0000 -0.0731 7.4983 0.0000 0.0000
3 4 261.9074 5.9533 0.0000 -0.6223 -0.3000 1.0000 36.0000 0.7275
  10.1541 -0.2366 29.7817 1.0000 -0.1083 8.5924 6.0658 0.0000
4 4 70.9120 54.0531 30.0000 0.4931 -0.3000 1.0000 16.0000 0.0392
  0.2476 -0.8055 7.1248 1.0000 -0.1009 8.7229 0.0000 0.0000

```

2	5	26.7569	0.0000	0.0000	1.0000	-0.3000	1.0000	36.0000	0.0100
		0.5785	-0.3500	25.0000	1.0000	-0.2601	6.6137	1.0000	0.0000
3	5	28.0000	0.0000	0.0000	0.4351	-0.3000	1.0000	36.0000	0.0656
		18.6859	-0.3500	25.0000	1.0000	-0.1391	7.4280	1.0000	0.0000
4	5	0.1000	0.0000	0.0000	0.2500	-0.5000	1.0000	35.0000	0.6000
		0.5000	-0.5000	20.0000	1.0000	-0.2000	10.0000	1.0000	0.0000
5	5	72.6003	0.0000	0.0000	-0.7273	0.3000	0.0000	25.0000	0.1919
		6.6441	-0.4000	12.0000	1.0000	-0.0345	5.0063	0.0000	0.0000
1	6	0.0000	0.0000	0.0000	-0.6528	-0.3000	0.0000	36.0000	0.5000
		10.0663	-0.3500	25.0000	1.0000	-0.1000	10.0000	0.0000	0.0000
2	6	92.8579	0.0000	0.0000	-0.6528	-0.3000	0.0000	36.0000	0.1551
		10.0663	-0.3500	25.0000	1.0000	-0.0842	7.1758	0.0000	0.0000
3	6	228.4876	0.0000	0.0000	-0.8524	-0.3000	0.0000	36.0000	0.1252
		0.4016	-0.3500	25.0000	1.0000	-0.1750	5.2102	0.0000	0.0000
4	6	0.0000	0.0000	0.0000	1.0000	0.3000	0.0000	26.0000	1.0000
		0.5000	0.0000	12.0000	1.0000	-0.2000	10.0000	0.0000	0.0000
5	6	0.1000	0.0000	0.0000	0.2500	-0.5000	1.0000	35.0000	0.6000
		0.5000	-0.5000	20.0000	1.0000	-0.2000	10.0000	1.0000	0.0000
6	6	34.0777	0.0000	0.0000	0.4832	-0.3000	0.0000	16.0000	0.5154
		6.4631	-0.4197	14.3085	1.0000	-0.1463	6.1608	0.0000	0.0000
13	! Nr of off-diagonal terms; Ediss;Ro;gamma;rsigma;rpi;rpi2								
1	2	0.1239	1.4004	9.8467	1.1210	-1.0000	-1.0000		
2	3	0.0283	1.2885	10.9190	0.9215	-1.0000	-1.0000		
1	3	0.0647	2.0109	10.0105	1.3177	1.2052	1.0682		
1	4	0.0541	2.0811	13.5179	1.7778	1.5840	-1.0000		
2	4	0.2000	1.5207	12.9535	1.2125	-1.0000	-1.0000		
3	4	0.2000	1.9048	10.8374	1.7163	1.2444	-1.0000		
2	5	0.1100	1.8410	9.1430	1.7735	-1.0000	-1.0000		
3	5	0.1497	1.5719	13.3058	1.6111	-1.0000	-1.0000		
4	5	0.1174	1.9434	17.1734	-1.0000	-1.0000	-1.0000		
1	6	0.2000	1.9000	12.0000	-1.0000	-1.0000	-1.0000		
2	6	0.0564	1.4937	12.0744	1.7276	-1.0000	-1.0000		
3	6	0.1651	1.8998	11.2212	1.5416	-1.0000	-1.0000		
4	6	0.0216	1.5025	11.8792	-1.0000	-1.0000	-1.0000		
58	! Nr of angles;at1;at2;at3;Thetao,o;ka;kb;pv1;pv2;val(bo)								
1	1	1	59.0573	30.7029	0.7606	0.0000	0.7180	6.2933	1.1244
1	1	2	65.7758	14.5234	6.2481	0.0000	0.5665	0.0000	1.6255
2	1	2	70.2607	25.2202	3.7312	0.0000	0.0050	0.0000	2.7500
1	2	2	0.0000	0.0000	6.0000	0.0000	0.0000	0.0000	1.0400
1	2	1	0.0000	3.4110	7.7350	0.0000	0.0000	0.0000	1.0400
2	2	2	0.0000	27.9213	5.8635	0.0000	0.0000	0.0000	1.0400
1	1	3	66.0686	28.5756	1.4793	0.0000	2.9950	58.6562	1.0000
3	1	3	84.3310	21.5172	5.4724	-1.0000	1.5183	0.0000	2.9776
2	1	3	64.3088	32.5434	2.1997	0.0000	0.1000	0.0000	1.2995
1	3	1	68.4903	45.0000	1.3617	0.0000	2.8294	0.0000	1.0000
1	3	3	80.6161	45.0000	1.4073	0.0000	1.0572	68.1072	1.4451
3	3	3	80.7324	30.4554	0.9953	0.0000	3.0000	50.0000	1.0783
1	3	2	90.0000	7.1513	7.5000	0.0000	1.3111	0.0000	3.0000
2	3	3	75.6935	50.0000	2.0000	0.0000	1.0000	0.0000	1.1680
2	3	2	85.8000	9.8453	2.2720	0.0000	2.8635	0.0000	1.5800
1	2	3	0.0000	8.9481	0.5983	0.0000	0.0000	0.0000	1.0000

3	2	3	0.0000	15.0000	2.8900	0.0000	0.0000	0.0000	2.8774
2	2	3	0.0000	8.5744	3.0000	0.0000	0.0000	0.0000	1.0421
4	4	4	78.5339	36.4328	1.0067	0.0000	0.1694	0.0000	1.6608
2	4	4	77.2616	5.0190	7.8944	0.0000	4.0000	0.0000	1.0400
2	4	2	75.7983	14.4132	2.8640	0.0000	4.0000	0.0000	1.0400
3	4	4	90.6812	31.1846	4.4543	0.0000	0.5073	0.0000	2.1809
2	4	3	73.6998	40.0000	1.8782	0.0000	4.0000	0.0000	1.1290
3	4	3	80.1361	36.2368	0.9504	0.0000	0.2624	0.0000	2.0787
4	3	4	80.4450	6.0739	1.7731	0.0000	3.2548	0.0000	1.0422
2	3	4	86.7611	7.1742	1.4013	0.0000	1.4999	0.0000	1.0400
3	3	4	103.4529	26.9589	1.3470	0.0000	1.7728	0.0000	1.3091
2	2	4	0.0000	47.1300	6.0000	0.0000	1.6371	0.0000	1.0400
4	2	4	0.0000	27.4206	6.0000	0.0000	1.6371	0.0000	1.0400
3	2	4	0.0000	5.0000	1.0000	0.0000	1.0000	0.0000	1.2500
1	1	4	72.5239	22.3583	2.0393	0.0000	1.0031	0.0000	1.0400
1	4	1	69.1709	18.9268	2.1226	0.0000	1.0031	0.0000	1.0400
4	1	4	68.6453	18.7377	2.0496	0.0000	1.0031	0.0000	1.0400
1	4	4	68.9902	19.7021	2.0587	0.0000	1.0031	0.0000	1.0400
2	1	4	72.6403	13.6964	2.4702	0.0000	1.0000	0.0000	1.0400
1	4	2	71.8708	14.6864	2.4702	0.0000	1.0000	0.0000	1.0400
1	3	4	85.8521	12.6881	1.0112	0.0000	1.0000	0.0000	1.3220
1	4	3	71.7524	35.8987	1.5000	0.0000	1.0000	0.0000	1.0487
3	1	4	70.0000	5.0250	1.0000	0.0000	1.0000	0.0000	1.2500
1	2	4	0.0000	2.5000	1.0000	0.0000	1.0000	0.0000	1.2500
3	5	3	100.0000	45.9627	3.0941	0.0000	3.2848	0.0000	2.0000
2	3	5	87.9313	7.1387	3.0639	0.0000	1.5000	0.0000	1.5554
5	3	5	84.9984	6.4965	1.5553	0.0000	1.0368	0.0000	2.0000
4	3	5	95.9867	2.0000	5.0000	0.0000	0.8452	0.0000	1.0000
3	2	6	0.0000	4.2750	1.0250	0.0000	1.3750	0.0000	1.4750
2	2	6	0.0000	3.0000	1.0000	0.0000	1.0000	0.0000	1.2500
6	2	6	0.0000	20.2391	0.1328	0.0000	2.9860	0.0000	1.0870
2	3	6	88.1144	13.2143	1.5068	0.0000	3.0000	0.0000	1.0100
3	3	6	34.4326	25.9544	5.1239	0.0000	2.7500	0.0000	1.7141
6	3	6	21.6945	20.0000	4.0000	0.0000	0.6619	0.0000	1.9714
2	6	2	67.4229	4.5148	5.9702	0.0000	3.0000	0.0000	2.6879
2	6	3	41.8108	17.3800	2.6618	0.0000	0.7372	0.0000	1.0100
3	6	3	49.1145	11.8902	2.1383	0.0000	3.0000	0.0000	1.4790
2	6	6	180.0000	-26.7860	7.3549	0.0000	1.0000	0.0000	1.0252
2	6	6	78.2279	37.6504	0.4809	0.0000	1.0000	0.0000	2.9475
4	3	6	16.5023	0.0100	2.7027	0.0000	1.0000	0.0000	1.0000
3	4	6	88.2703	0.3954	0.2500	0.0000	0.5000	0.0000	2.1060
3	6	4	83.8306	0.3712	0.2500	0.0000	0.5000	0.0000	2.1153
31	! Nr of torsions;at1;at2;at3;at4;;V1;V2;V3;V2(BO);vconj;n.u;n								
1	1	1	1	-0.2500	34.7453	0.0288	-6.3507	-1.6000	0.0000
1	1	1	2	-0.2500	29.2131	0.2945	-4.9581	-2.1802	0.0000
2	1	1	2	-0.2500	31.2081	0.4539	-4.8923	-2.2677	0.0000
1	1	1	3	-0.5740	22.4215	0.8787	-2.7603	-1.1000	0.0000
2	1	1	3	1.8164	18.8479	0.5134	-7.0513	-1.0978	0.0000
3	1	1	3	-2.5000	56.1599	-1.0000	-4.3607	-0.8614	0.0000
1	1	3	1	2.5000	14.6490	1.0000	-2.5209	-0.9000	0.0000
1	1	3	3	-0.0002	20.1851	0.1601	-9.0000	-2.0000	0.0000

1	3	3	1	0.0002	80.0000	-1.5000	-4.4848	-2.0000	0.0000	0.0000
3	1	3	3	-0.1583	20.0000	1.5000	-9.0000	-2.0000	0.0000	0.0000
1	1	3	2	-2.2946	11.6826	-1.0000	-2.5000	-0.9000	0.0000	0.0000
2	1	3	1	-1.0402	26.8401	0.6384	-2.5000	-0.9000	0.0000	0.0000
2	1	3	2	-1.0000	66.0304	0.7580	-5.4593	-1.1000	0.0000	0.0000
2	1	3	3	2.1531	45.9655	1.0000	-2.5000	-2.8274	0.0000	0.0000
3	1	3	1	0.6706	80.0000	-0.2443	-4.7181	-3.0437	0.0000	0.0000
3	1	3	2	-1.0000	91.6742	-0.5000	-3.9849	-3.0476	0.0000	0.0000
1	3	3	2	-2.5000	-0.5181	0.0268	-5.4085	-2.9498	0.0000	0.0000
2	3	3	2	-2.1995	-25.0000	-1.0000	-2.6000	-0.9921	0.0000	0.0000
1	3	3	3	2.4118	-24.8219	0.9706	-2.5004	-0.9972	0.0000	0.0000
2	3	3	3	-2.5000	43.1840	-0.6826	-6.6539	-1.2407	0.0000	0.0000
3	3	3	3	-2.5000	-25.0000	1.0000	-2.5000	-0.9000	0.0000	0.0000
0	1	2	0	0.0000	0.0000	0.0000	0.0000	0.0000	0.0000	0.0000
0	2	2	0	0.0000	0.0000	0.0000	0.0000	0.0000	0.0000	0.0000
0	2	3	0	0.0000	0.1000	0.0200	-2.5415	0.0000	0.0000	0.0000
0	1	1	0	0.0000	50.0000	0.3000	-4.0000	-2.0000	0.0000	0.0000
0	3	3	0	0.5511	25.4150	1.1330	-5.1903	-1.0000	0.0000	0.0000
2	4	4	2	0.0000	0.0000	0.0640	-2.4426	0.0000	0.0000	0.0000
2	4	4	4	0.0000	0.0000	0.1587	-2.4426	0.0000	0.0000	0.0000
0	2	4	0	0.0000	0.0000	0.1200	-2.4847	0.0000	0.0000	0.0000
3	1	1	4	-0.5740	22.4215	0.8787	-2.7603	-1.1000	0.0000	0.0000
1	1	4	3	-0.5740	22.4215	0.8787	-2.7603	-1.1000	0.0000	0.0000
1	! Nr of hydrogen bonds;at1;at2;at3;Rhb;Dehb;vhb1									
3	2	3		2.1200	-3.5800	1.4500	19.5000			

Reference:

1. K. Vollmayr, W. Kob, and K. Binder, "Cooling-rate effects in amorphous silica: A computer-simulation study," *Physical Review B*, 54[22] 15808 (1996).
2. A. Tilocca, "Cooling rate and size effects on the medium-range structure of multicomponent oxide glasses simulated by molecular dynamics," *The Journal of chemical physics*, 139[11] 114501 (2013).
3. J. M. D. Lane, "Cooling rate and stress relaxation in silica melts and glasses via microsecond molecular dynamics," *Physical Review E*, 92[1] 012320 (2015).
4. L. Deng and J. Du, "Effects of system size and cooling rate on the structure and properties of sodium borosilicate glasses from molecular dynamics simulations," *The Journal of chemical physics*, 148[2] 024504 (2018).
5. S. Plimpton, "Fast parallel algorithms for short-range molecular dynamics," *Journal of computational physics*, 117[1] 1-19 (1995).
6. J. Banerjee, S. H. Kim, and C. G. Pantano, "Elemental areal density calculation and oxygen speciation for flat glass surfaces using x-ray photoelectron spectroscopy," *Journal of Non-Crystalline Solids*, 450 185-93 (2016).
7. S. H. Hahn, J. Rimsza, L. Criscenti, W. Sun, L. Deng, J. Du, T. Liang, S. B. Sinnott, and A. C. Van Duin, "Development of a ReaxFF Reactive Force Field for NaSiO_x/Water Systems and Its Application to Sodium and Proton Self-Diffusion," *The Journal of Physical Chemistry C*, 122[34] 19613-24 (2018).
8. H. Strandh, L. G. Pettersson, L. Sjöberg, and U. Wahlgren, "Quantum chemical studies of the effects on silicate mineral dissolution rates by adsorption of alkali metals," *Geochim Cosmochim Acta*, 61[13] 2577-87 (1997).
9. Y. Xiao and A. C. Lasaga, "Ab initio quantum mechanical studies of the kinetics and mechanisms of silicate dissolution: H⁺ (H₃O⁺) catalysis," *Geochim Cosmochim Acta*, 58[24] 5379-400 (1994).
10. I. S. Flyagina, A. I. Malkin, and S. P. Dolin, "Quantum-chemical simulation of the adsorption-induced reduction of strength of siloxane bonds," *Journal of molecular modeling*, 25[6] 161 (2019).